

https://dspace.org/

An algorithm for the automatic resolution of the position, orientation and dipole moment of a magnetic dipole antenna buried in rock

Lishman, Ryan M

2008-05-05T07:29:42Z
http://hdl.handle.net/10539/4781

Downloaded from a DSpace repository. https://dspace.org/

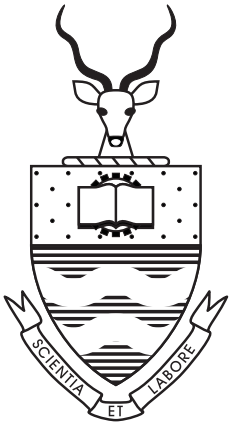

UNIVERSITY
OF THE
WITWATERSRAND
JOHANNESBURG

An Algorithm for the Automatic Resolution of the Position, Orientation and Dipole Moment of a Magnetic Dipole Antenna Buried in Rock

Ryan M. Lishman

A dissertation submitted to the Faculty of Engineering and the Built Environment, University of the Witwatersrand, Johannesburg, in partial fulfilment of the requirements for the degree of Master of Science in Engineering.

Johannesburg, April 2004

Declaration

I declare that this is my own, unaided work, except where otherwise indicated. It is being submitted for the degree of Master of Science in Engineering at the University of the Witwatersrand, Johannesburg. It has not been submitted before for any degree or examination at any other university. The early part of this work was completed while I was employed by the CSIR division of Mining Technology.

Signed this _____ day of _____ 2004

_____

Ryan M. Lishman.

Abstract

In this paper, an algorithm for accurately finding the position, orientation and dipole moment of a transmitting dipole antenna buried in rock is presented. The algorithm is based on simplified radiation equations that are shown to be valid within a region of space in the extreme near field surrounding the antenna called termed quasi-static region. Within this region, medium dependent propagation effects are negligible, allowing accurate, medium independent resolution of position, orientation and dipole moment.

The magnetic field magnitude and direction values observed at a number of arbitrarily located points in space are used by the algorithm to generate a system of nonlinear equations. This system of equations is solved using a simultaneous multi-variable Newton-Raphson solver with line searches and backtracking providing a measure of global convergence. An additional method, based on an iterated random search, further improves the global convergence capability of the algorithm.

If the dipole moment of the transmitting antenna is known, measurements from two observer points are sufficient to resolve the position and orientation of the dipole. If the dipole moment is unknown, three observer points are required to solve for the unknown position, orientation and dipole moment. The algorithm is able to find an exact solution using exact theoretical measurements, and a minimised least squares solution where measurements are subject to noise.

The theory relating to the algorithm is discussed including distance-frequency relations for the quasi-static region of a number of common rock types. Probabilistic modelling, simulation and test results of the algorithm are also included.

For my El Shadi, you're more than enough.

Acknowledgements

I would like to acknowledge the help of my supervisor, Alan Clark, for his guidance and “savvy” advice over the past two years. I am also greatly indebted to Declan Vogt for his guidance in many areas relating to this research, especially those of through-rock electromagnetic wave propagation and genetic algorithms.

I must thank the CSIR division of Mining Technology, and particularly Valery Kononov, for introducing me to field of through earth location techniques. Much of my early research into this field came as a result of a multitude of thought provoking and inspiring discussions with Valery. The practical validation and testing of this algorithm would also not have been possible without the help of the technicians at the CSIR, Reinhard Bilgeri and Karlo Walker, for whom nothing was too much to ask.

Lastly, thanks must go to my “stats mate”, Stephen Davis, for his superbly willing guidance and gentle correction in the area of statistics relating to the algorithm.

Foreword

This research report introduces a topic that at first glance, seems both arbitrary and abstract. The ability to resolve the unknown location, orientation and dipole moment of a source does, however, hold significant practical benefit. Chief among these is the benefit offered to the mining and tunnelling industries, where solutions to problems such as trapped personnel location, tunnel end location and other general problems such as locating "lost" boreholes are made available.

Depending on the practical accuracy of the method, the implementation of a similar system to the terrestrial Global Positioning System (GPS) for underground environments may even be possible. In environments such as mines and tunnels, where the high frequency signals used in the conventional GPS system are unable to propagate through the conductive rock, this offers significant gain.

The approach chosen for the layout of this research report is that of a concise theoretical paper outlining the key postulates and findings, backed up by supporting appendices of a more tutorial nature. The intention of this approach is to allow the submission of the paper forming the body of this report to a recognised journal without excessive amendment. As such, in reading this report, an author unfamiliar with the topics of EM propagation through rock and mathematical minimisation may have to consult the appendices more frequently than a report of a more conventional style. I offer my apologies for this inconvenience.

Section I introduces the algorithm and its application, and provides a summary of the available literature relating to this and other similar fields.

Section II describes the quasi-static region, outlining the simplified radiation equations for the magnetic dipole that are valid with the region.

Section III systematically describes the formulation of the algorithm. The three basis equations that allow the formation of the system of nonlinear equations are discussed as well as the necessary geometric transformations required to apply the basis equations to the general case. The modified Newton-Raphson algorithm is described in III-C. A method that further improves on this algorithm is described in III-D.

Section IV characterises the performance of the algorithm both in the ideal noiseless case and in the case when noisy measurements are used. Probabilistic modeling of the algorithms is shown in IV-B. Practical field tests and their results are given in IV-D.

Section V discusses the conclusions of the study and recommendations for further work in this field.

Table of Contents

Abstract iii

Acknowledgements v

Foreword vi

Table of Contents vii

List of Figures ix

List of Tables x

Paper: An Algorithm for the Automatic Resolution of the Position, Orientation and Dipole Moment of a Magnetic Dipole Antenna Buried in Rock 1

I Introduction 1

II The "quasi-static region" 2

III Formulation of the algorithm 3
- III-A The basis equations underlying the methodology . . . 3
- III-B Formulation of the system of nonlinear equations . . . 3
- III-C Finding the unknown antenna parameters using a modified Newton-Raphson algorithm . . . 4
- III-D Globalising the search for the unknown antenna parameters . . . 5

IV Simulation and testing 6
- IV-A Simulation methodology . . . 6
- IV-B Probability model of the algorithm . . . 6
- IV-C Simulation of the algorithms using measurements subject to noise . . . 6
- IV-D Field testing of the algorithm . . . 6

V Conclusion and recommendations for further work 8

References 8

Appendix A: Derivation of the E and H fields for an electrically small loop antenna 10
- A-1 Describing **E** and **H** in terms of **A** for a conductive medium . . . 10
- A-2 Derivation of the **E** and **H** fields of a small circular loop in a conductive medium 11

Appendix B: EM wave propagation in rock 14

Appendix C: A background to geometric transformations 20
- C-1 Derivation of the rotation angles, β_y and β_x, for a given set of spherical angles 20
- C-2 Rotation of spherical angles (θ_1, ϕ_1) to (θ_2, ϕ_2) . . . 21

Appendix D: The Newton-Raphson algorithm with line searches and backtracking 23

Appendix E: A formal description of the location algorithm 26

Appendix F: Contemporary global minimisation algorithms attempted in the search for the unknown antenna parameters 28
F-1 Genetic Algorithm 28
F-2 Simulated annealing 30

Appendix G: Probabilistic modelling of the algorithm) 32

Appendix H: Simulated results of the algorithm using measurements subject to noise 35

Appendix References 37

List of Figures

1 The ratio of the magnetic field produced by a magnetic dipole on the surface of a uniform half space to that of a dipole in free space vs the response parameter, ζ (after [3]). 2
2 The dimension of the quasi-static region of a number of common rock types 3
3 The magnitude and direction of the magnetic field vector, **H**, relative to the coordinate system 3
4 The number of trials required for a correct solution to be found to a certain confidence for varying numbers of observer points 7
5 The error in predicted position, orientation and dipole moment for increasing values of measurement noise (dipole moment unknown). 7
6 The error in predicted position and orientation for increasing values of measurement noise (dipole moment known). 7
7 The error in position and orientation between predicted and known values during field testing for random combinations of up to 13 observer points. 7
8 The configuration of the small circular loop (after [3]). 12
9 The conductivity and relative permittivity of a number of common rock types calculated from Debye models with multiple relaxation times. 19
10 Finding the rotation angles β_y and β_x for a given set of spherical angles. 21
11 The distribution of iterations between correct outcomes of the algorithm for one random configuration of antenna parameters and observer points. 33
12 The empirical and cumulative distributions of the number of trials of the algorithm required for a correct solution for an arbitrary configuration of antenna parameters and observer points. 34
13 The error in predicted position and orientation for increasing values of measurement noise (two observer points, dipole moment known). 35
14 The error in predicted position, orientation and dipole moment for increasing values of measurement noise (three observer points, dipole moment unknown). 35
15 The error in predicted position and orientation for increasing values of measurement noise (three observer points, dipole moment known). 35
16 The error in predicted position, orientation and dipole moment for increasing values of measurement noise (five observer points, dipole moment unknown). 36
17 The error in predicted position and orientation for increasing values of measurement noise (five observer points, dipole moment known). 36
18 The error in predicted position, orientation and dipole moment for increasing values of measurement noise (ten observer points, dipole moment unknown). 36
19 The error in predicted position and orientation for increasing values of measurement noise (ten observer points, dipole moment known). 36

List of Tables

I Approximate attenuation constant, phase constants and skin depth for good conductors and dielectrics 17

An Algorithm for the Automatic Resolution of the Position, Orientation and Dipole Moment of a Magnetic Dipole Antenna Buried in Rock

Ryan M. Lishman

***Abstract*—In this paper, an algorithm for accurately finding the position, orientation and dipole moment of a transmitting dipole antenna buried in rock is presented. The algorithm is based on simplified radiation equations that are shown to be valid within a region of space in the extreme near field surrounding the antenna called termed quasi-static region. Within this region, medium dependent propagation effects are negligible, allowing accurate, medium independent resolution of position, orientation and dipole moment.**

The magnetic field magnitude and direction values observed at a number of arbitrarily located points in space are used by the algorithm to generate a system of nonlinear equations. This system of equations is solved using a simultaneous multi-variable Newton-Raphson solver with line searches and backtracking providing a measure of global convergence. An additional method, based on an iterated random search, further improves the global convergence capability of the algorithm.

If the dipole moment of the transmitting antenna is known, measurements from two observer points are sufficient to resolve the position and orientation of the dipole. If the dipole moment is unknown, three observer points are required to solve for the unknown position, orientation and dipole moment. The algorithm is able to find an exact solution using exact theoretical measurements, and a minimised least squares solution where measurements are subject to noise.

The theory relating to the algorithm is discussed including distance-frequency relations for the quasi-static region of a number of common rock types. Probabilistic modelling, simulation and test results of the algorithm are also included.

I. Introduction

THIS this paper considers the problem of locating and determining the orientation and dipole moment of a magnetic dipole antenna buried in rock. This problem occurs in many practical underground situations, the most common of these being the location of miners trapped under rock-falls and "lost boreholes", and has previously been solved using field gradient and triangulation techniques. Such approaches suffer, however, from an inherent degree of uncertainty due to the non-spherical nature of the dipole's radiated magnetic field strength in the near field. The polarisation of the radiated field also introduces additional uncertainty to these techniques.

This paper describes another approach to the problem that numerically solves for the dipole's position, orientation and dipole moment based on its theoretical radiation characteristics in the near field and the magnitude and direction of the magnetic field measured at a number of arbitrary observer points whose position is known. In practice, the magnitude and direction of the magnetic field can be measured using a number of methods, the most common of these being through the use of an orthogonal, triaxial receiving loop antenna system.

The presence of the heterogeneous conductive rock environment surrounding the dipole constrains the area within which it can be accurately located to a region who's dimensions are inversely proportional to the frequency of the radiated signal. Estimates of the electrical rock properties allow the calculation of this region, termed the "quasi-static region". Within this quasi-static region, the algorithm will perform reliably, suffering negligible conductive losses and medium-dependant effects. The frequency of operation of the system yielding a usable quasi-static region is typically in the Very Low Frequency (VLF) band.

The effect of a finitely conducting medium on the propagation of electromagnetic (EM) waves was initially considered by Sommerfeld in as early as 1909 [1]. Since then, a sizable array of literature on the subjects of EM wave propagation in a conductive medium and subsurface EM wave propagation has appeared. Noteworthy contributions among these include the ground-breaking work done in 1949 by Wadley [2], who measured and determined a model describing the attenuation of EM waves through rock, work done by Wait [3], [4] on determining the fields of a magnetic dipole in nonhomogeneous conducting media, and a summary of low frequency EM propagation in conductive media made by Kraichman [5]. An excellent review of subsurface EM wave propagation was conducted by Gabillard et al. [4] in 1973. These contributions are by no means the only significant ones. In fact, such is the vastness of research related to subsurface EM wave propagation that it would seem impossible to conduct further research in this field.

The field of underground location and position finding is a little less researched. Efforts into the location of underground radio transmitters began in the early 1970s with the US Bureau of Mines conducting theoretical and practical investigations into the location of a buried transmitter using a receiver on the surface [7], [8]. A number of systems were developed around this concept by the US Bureau of Mines. At the same time, in Europe, a number of short range EM location systems were developed, using field gradient and triangulation techniques.

A location technique based on the relationship between the magnitude of the magnetic field and the distance from the source was first considered by Nessler [9], who required four observer points to locate the source. Further work by Nessler includes the use of an auxiliary source antenna to enable the observer points to identify their location [10]. The algorithm described in this paper improves on Nessler's technique by applying both a magnitude and direction constraint to the magnetic dipole source to obtain more than one nonlinear equation for each observer point, requiring less observer points to locate

R. M. Lishman is an MSc student at the School of Electrical and Information Engineering of the University of the Witwatersrand, Johannesburg, South Africa (email: ryan@embedded-iq.com)

the source, as well as yielding the orientation of the source.

If the applied dipole moment of the transmitting antenna is known, measurements from only two observer points are sufficient to resolve the position and orientation of the dipole. If unknown, three observer points are required to resolve the position, orientation and dipole moment of the dipole.

II. The "quasi-static region"

In practice, a magnetic dipole may be approximated using a loop antenna whose diameter is small when compared with the free-space wavelength. The electric and magnetic fields of an electrically small loop antenna in a homogeneous medium of constitutive parameters μ, ϵ and σ are widely known. Derivations of these fields from first principles can be found in [11, Appendix A] and are given in spherical coordinates by the following relations[1]:

$$H_r = \frac{NIA\cos\theta}{2\pi r^3}\left[1+\gamma r\right]e^{-\gamma r} \tag{1}$$

$$H_\theta = \frac{NIA\sin\theta}{4\pi r^3}\left[1+\gamma r-(\gamma r)^2\right]e^{-\gamma r} \tag{2}$$

$$E_\phi = -\frac{j\omega\mu NIA\sin\theta}{4\pi r^2}\left[1+\gamma r\right]e^{-\gamma r} \tag{3}$$

$$H_\phi = E_r = E_\theta = 0 \tag{4}$$

where N is the number of turns comprising the loop antenna, I is the current in the loop, A is the area enclosed by the loop, ω is the angular frequency and γ, the propagation constant given, for a conductive medium, by the well known relation:

$$\gamma = \sqrt{j\omega\mu\sigma-\omega^2\mu\epsilon} = \alpha + j\beta \tag{5}$$

In (5), γ consists of a real attenuation component and an imaginary phase component given by:

$$\alpha = \omega\sqrt{\mu\epsilon}\left\{\frac{1}{2}\left[\sqrt{1+\left\{\frac{\sigma}{\omega\epsilon}\right\}^2}-1\right]\right\}^{\frac{1}{2}} \tag{6}$$

$$\beta = \omega\sqrt{\mu\epsilon}\left\{\frac{1}{2}\left[\sqrt{1+\left\{\frac{\sigma}{\omega\epsilon}\right\}^2}+1\right]\right\}^{\frac{1}{2}} \tag{7}$$

For small values of $|\gamma r|$, the $e^{-\gamma r}$ term in (1) and (2) can be expanded in a Maclaurin series to yield the following:

$$e^{-\gamma r} = 1-\gamma r+\frac{1}{2}(\gamma r)^2-\ldots \tag{8}$$

Substituting this expansion into (1) and (2) yields:

$$H_r = \frac{NIA\cos\theta}{2\pi r^3}\left[1-\frac{1}{2}(\gamma r)^2+\ldots\right] \tag{9}$$

$$H_\theta = \frac{NIA\sin\theta}{4\pi r^3}\left[1-\frac{3}{2}(\gamma r)^2+\ldots\right] \tag{10}$$

[1]All physical quantities are assumed to be represented in SI units, unless otherwise specified.

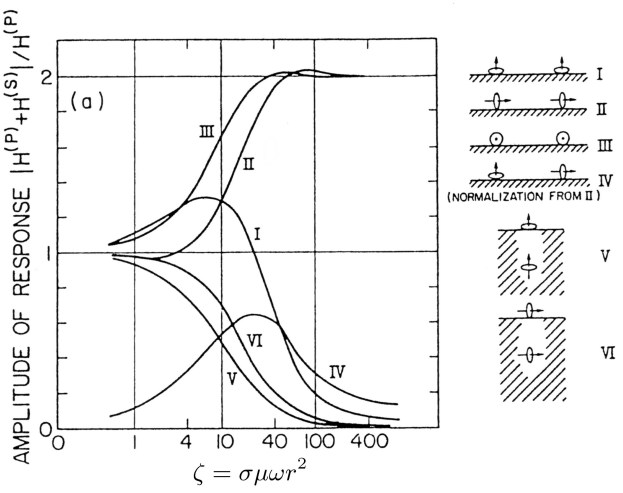

Fig. 1. The ratio of the magnetic field produced by a magnetic dipole on the surface of a uniform half space to that of a dipole in free space vs the response parameter, ζ (after [3]).

For values of ω and r such that $|(\gamma r)^2| \ll 1$, the magnetic field described by (9) and (10) is effectively "medium independent", in that it no longer depends on the conductivity and electric permittivity of the medium.

Since $|(\gamma r)^2| = |\gamma|^2 r^2$ and $|\gamma|^2 = \alpha^2+\beta^2$, a region may be defined, within which, the fields of the dipole are quasi-stationary. This "quasi-static region" is described by the following relation:

$$r^2\omega^2\mu\epsilon\sqrt{1+\left(\frac{\sigma}{\omega\epsilon}\right)^2} \ll 1 \tag{11}$$

If the medium is a good dielectric at the frequency of operation ($\sigma \ll \omega\epsilon$), the region described by (11) can be recognised as being equivalent to the near field region of the dipole antenna in free space. However, when the conductive currents in the medium dominate, the quasi-static region can be significantly smaller than the near field region. In (11), the term under the square root denotes this "shortening" factor.

Although this description of a "quasi-static region" is based on a homogeneous model, significant evidence supporting its existence in a heterogeneous medium may be found. The most obvious of these is Wait's consideration of the fields created by a magnetic dipole situated on the surface of a uniform half space [3][2]. A dipole situated on the surface of a uniform half space can be considered a severe inhomogeneity in the medium. Wait's results are shown in Fig. 1, where he describes the ratio of fields produced by a magnetic dipole situated on the surface of the half space to those produced by an equivalent dipole in free space.

Figure 1 shows that for values of $\zeta \ll 1$, the fields of the dipole situated on the surface of the half space are approximately equal to those of an equivalent dipole in free space.

Wait describes the fields in terms of a response parameter, $\zeta = \sigma\mu\omega r^2$, which is the same as that given in the left hand side of (11) for the case when the conduction currents dominate the displacement currents[3].

[2]A uniform half space can be considered to be an infinite region in space where exactly half of region is made up of a medium of constitutive parameters μ, ϵ and σ and the other half of the region is free space, having constitutive parameters μ_0, ϵ_0 and $\sigma = 0$.

[3]In his analysis, Wait neglects all displacement currents. One can see that

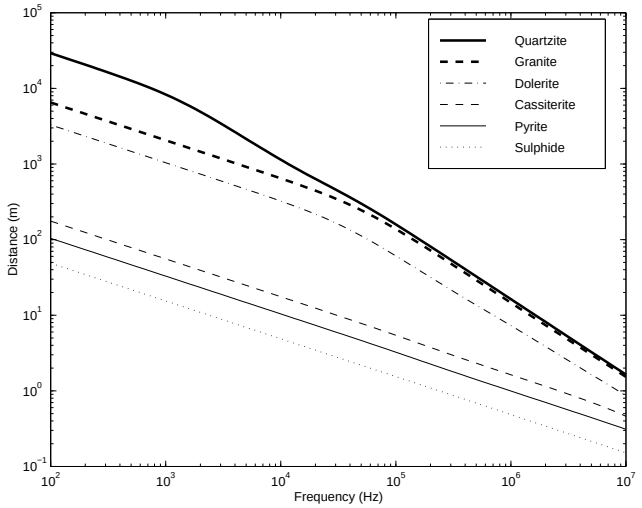

Fig. 2. The dimension of the quasi-static region of a number of common rock types

Although no analysis is given to prove the existence of a quasi-static region in an anisotropic medium, it is reasonable to assume that one does exist.

The dimension of the quasi-static region at various frequencies may be found by substituting for the constitutive parameters of the surrounding rock into (11). Vogt, in [5], derives frequency dependant models for rock constitutive parameters by fitting a Debye model with multiple relaxation times to his measured data, allowing the dispersive nature of many common rock types to be accounted for. The generalisation of Vogt's Debye models, as well as a background to the propagation of EM waves in rock is given in [11, Appendix B].

Taking the boundary of the quasi-static region to be the point at which the "medium independent" components of the magnetic field equal the "medium dependent" components, and substituting the Debye predicted constitutive parameters into (11), a relation for the dimension of the quasi-static region to frequency for a number of common rock types is shown in Fig. 2.

Figure 2 shows that the frequency of operation required for a meaningful dimension of quasi-static region falls in the Low Frequency (LF) to Very Low Frequency (VLF) range. At these frequencies, the electric field, given by (e:Ep) is negligible when compared to the magnetic field, and is henceforth omitted in the development of the location algorithm.

III. Formulation of the Algorithm

A. The basis equations underlying the methodology

Assume that a magnetic dipole source is situated at the origin of a right hand coordinate system with the dipole aligned with the z-axis of the coordinate system. Within the quasi-static region, the spherical components of the magnetic field can be approximated by the following relations:

$$H_r \approx \frac{NIA\cos\theta}{2\pi r^3} \tag{12}$$

$$H_\theta \approx \frac{NIA\sin\theta}{4\pi r^3} \tag{13}$$

Wait's response parameter, ζ, equals the left hand side of (11) as $\omega\epsilon \to 0$, so the response parameters are effectively identical.

$$H_\phi = 0 \tag{14}$$

The magnitude of the magnetic field is the vector sum of the components, given as:

$$|\mathbf{H}| = \frac{NIA}{4\pi r^3}\sqrt{1+3\cos^2\theta} \tag{15}$$

The direction of $\mathbf{H}$ is not a function of ϕ, so the horizontal spherical angle of $\mathbf{H}$ is simply given by:

$$\phi_H = \phi \tag{16}$$

The angle of $\mathbf{H}$ with respect to the radius vector, shown in Fig. 3 and denoted ψ, is given by:

$$\tan\psi = \frac{H_\theta}{H_r} = \frac{1}{2}\tan\theta \tag{17}$$

From (17), as shown in Fig. 3, the vertical spherical angle of the magnetic field, θ_H, can be expressed as:

$$\begin{aligned}\theta_H = \theta + \psi &= \arctan\left[\frac{3\tan\theta}{2-\tan^2\theta}\right] \\ &= \arctan\left[\frac{3\sin 2\theta}{3\cos 2\theta + 1}\right]\end{aligned} \tag{18}$$

B. Formulation of the system of nonlinear equations

Equations (15), (16) and (18) are the basis equations used in forming the system of nonlinear equations. In order to apply these equations describing a dipole situated at the origin and oriented along the z-axis to one of arbitrary position and orientation, a geometric translational and rotational transformation is applied. The subject of geometric transformations is given an extensive treatment in [11, Appendix C].

Assume the magnetic dipole is located at a point within the quasi-static region given by $\mathbf{p}_d(x_d, y_d, z_d)$ within the global coordinate system. A local coordinate system who's axes are parallel to those of the global coordinate system is assumed to exist such that the dipole is situated at its origin. The axis of the

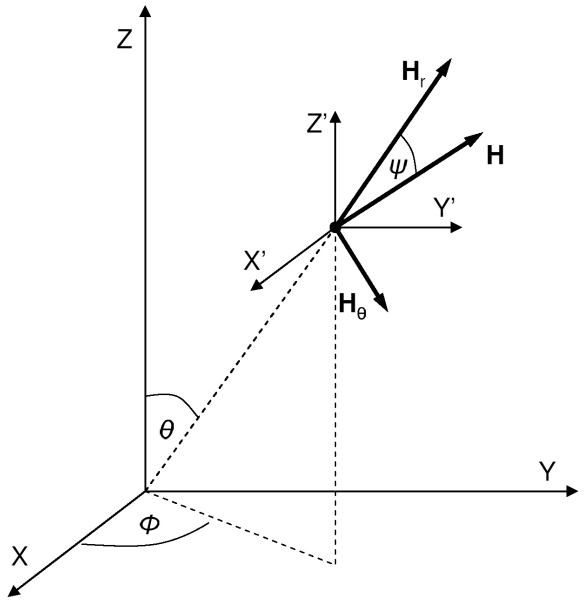

Fig. 3. The magnitude and direction of the magnetic field vector, $\mathbf{H}$, relative to the coordinate system

dipole is assumed to be orientated along a ray emanating outward from the origin of the local coordinate system at spherical angles[4] (θ_d, ϕ_d).

Assume also, that a number of distinct points of reception, N, exist whose coordinates as well as received magnetic field magnitude and direction are known. Each of these observer points has the coordinates $\mathbf{p}_i(x_i, y_i, z_i)$, a magnetic field magnitude of $|\mathbf{H}_i|$ and spherical angles of the received magnetic field vector (θ_i, ϕ_i) relative to the local coordinate system.

In order to satisfy the basis equations (15), (16) and (18), the following geometric transformations are made:

1) Firstly, each point $\mathbf{p}_i$ is translated by $-\mathbf{p}_d$. This has the effect of translating (shifting) the magnetic dipole to the origin of the global coordinate system.
2) Secondly, each point $\mathbf{p}_i$ is rotated about the origin by $-(\theta_d, \phi_d)$. This has the effect of orientating the axis of the magnetic dipole along the z-axis of the global coordinate system. The transformed (translated and rotated) point is denoted $\mathbf{p}_i^*(x_i^*, y_i^*, z_i^*)$.
3) Thirdly, each set of spherical angles (θ_i, ϕ_i) is also rotated about the origin by $-(\theta_d, \phi_d)$. The transformed (rotated) angles are denoted (θ_i^*, ϕ_i^*).

The three basis equations are satisfied when the measured value of $|\mathbf{H}_i|$ and the transformed measured spherical angles, (θ_i^*, ϕ_i^*), are substituted into the left hand sides of (15), (16) and (18) respectively. The right hand sides of (15), (16) and (18) are formed by substituting the following values for r, θ and ϕ:

$$r = \sqrt{(x_i^*)^2 + (y_i^*)^2 + (z_i^*)^2} \tag{19}$$

$$\theta = \arccos\left(\sqrt{\frac{(z_i^*)^2}{(x_i^*)^2 + (y_i^*)^2}}\right) \tag{20}$$

$$\phi = \arctan\left(\frac{y_i^*}{x_i^*}\right) \tag{21}$$

While the task of translating the observer points by $-\mathbf{p}_d$ is trivial, that of rotating them by $-(\theta_d, \phi_d)$ is more complex. This rotational transformation can be simplified by converting the spherical rotation angles into a rectangular rotation angles, $-(\beta_y, \beta_x)$. This rectangular rotation implies the rotation of each observer point first about the x-axis by $-\beta_x$ and second about the y-axis by $-\beta_y$. Expressions for β_x and β_y in terms of spherical angles are as follows:

$$\begin{bmatrix} \beta_x \\ \beta_y \end{bmatrix} = \begin{bmatrix} \arctan\left(-\dfrac{\sin\theta_d \sin\phi_d}{\cos\theta_d}\right) \\ \arcsin\left(\sin\theta_d \cos\phi_d\right) \end{bmatrix} \tag{22}$$

Once β_x and β_y have been determined, the transformed point $\mathbf{p}_i^*$ is given as:

$$\begin{bmatrix} x_i^* \\ y_i^* \\ z_i^* \end{bmatrix} = \mathbf{R}_{xy} \begin{bmatrix} x_i \\ y_i \\ z_i \end{bmatrix} - \begin{bmatrix} x_d \\ y_d \\ z_d \end{bmatrix} \tag{23}$$

where the rotation matrix, $\mathbf{R}_{xy}$, is given by :

[4]This is equivalent to saying that, were the dipole to be translated to the origin of the global coordinate system, the axis of the dipole would be orientated along a ray emanating outward from the origin of the global coordinate system at spherical angles (θ_d, ϕ_d).

$$\mathbf{R}_{xy} = \begin{bmatrix} \cos\beta_y & \sin\beta_x \sin\beta_y & -\cos\beta_x \sin\beta_y \\ 0 & \cos\beta_x & \sin\beta_x \\ \sin\beta_y & -\sin\beta_x \cos\beta_y & \cos\beta_x \cos\beta_y \end{bmatrix} \tag{24}$$

Rotating each set of spherical angles (θ_i, ϕ_i) first around the x-axis by $-\beta_x$ and then around the y-axis by $-\beta_y$, the following expressions for θ_i^* and ϕ_i^* are obtained:

$$\mathbf{S} = \begin{bmatrix} \sin\theta_i^* \cos\phi_i^* \\ \sin\theta_i^* \sin\phi_i^* \\ \cos\theta_i^* \end{bmatrix} = \mathbf{R}_{xy} \begin{bmatrix} \sin\theta_i \cos\phi_i \\ \sin\theta_i \sin\phi_i \\ \cos\theta_i \end{bmatrix} \tag{25}$$

$$\theta_i^* = \arccos\left(S_3\right) \tag{26}$$

$$\phi_i^* = \arctan\left(\frac{S_2}{S_1}\right) \tag{27}$$

C. Finding the unknown antenna parameters using a modified Newton-Raphson algorithm

For N observer points, a $3N$ system of nonlinear equations of the following form is obtained:

$$\mathbf{F}(\mathbf{x}) = 0 \tag{28}$$

where $\mathbf{x} = [x_d, y_d, z_d, \theta_d, \phi_d, NIA]$ is the vector of unknowns denoting the position, orientation and dipole moment of the magnetic dipole. It is fairly obvious that an empirical solution to (28) would be extremely difficult if not impossible to find. However, assuming a sufficient number of observer points are available, the system of equations can be solved numerically using an appropriate iterative method.

The method prescribed for the solution of (28) is a variant of the conventional Newton-Raphson method and employs line-searches and back-tracking. A detailed description of the algorithm is found in [11, Appendix D], while [8] contains an excellent treatment on this and other classical algorithms for solving systems of nonlinear equations. A common view held is that if the function $\mathbf{F}(\mathbf{x})$ and its derivatives are able to be evaluated at relatively low computational cost and one has a sufficiently good initial guess as to the solution, the Newton-Raphson method and its variants have definite advantages over other competing methods, chief among these being the quadratic convergence to a solution of the algorithm in the neighbourhood of a solution.

Like all Newton-Raphson variants, the algorithm is iterative and, given an initial starting vector, improves on the solution after the kth iteration using the following formula:

$$\mathbf{x}_{k+1} = \mathbf{x}_k + \lambda\delta\mathbf{x}, \qquad 0 < \lambda \leq 1 \tag{29}$$

The update term, $\delta\mathbf{x}$ is given in terms of the Jacobian matrix, $\mathbf{J}$, by:

$$\delta\mathbf{x} = -\mathbf{J}(\mathbf{x})^{-1}\mathbf{F}(\mathbf{x}_k) \tag{30}$$

Equation (30) can be solved by *QR* decomposition or singular value decomposition. If more than two points of reception exist, the system is over specified and, while a unique solution will still exist, (30) will give the value for $\delta\mathbf{x}$ in a least squares sense.

It is more computationally efficient to obtain the Jacobian matrix, $\mathbf{J}$, by using a finite difference approximation than by obtaining and empirical expression for it. This comes at no cost to the algorithm, since, as demonstrated by Dennis and Schnabel [8], the quadratic convergence properties of the Newton-Raphson method can be retained using a finite difference approximation to the Jacobian matrix for a properly chosen difference size. A finite difference approximation to $\mathbf{J}$ can be expressed as:

$$J_{ij}(x_j) \approx \frac{F_i(x_j + h) - F_i(x_j)}{h} \tag{31}$$

where the other elements of $\mathbf{x}$ besides x_j are assumed constant and the difference size is given as h. For an expected value of $J_{ij} \approx 1$, a value of h as the square root of the machine precision gives the most accurate approximation.

In order to perform an iteration of (29), the value of λ is subject to the following constraints applied to an objective function formed in terms of the scalar length of $\mathbf{F}(\mathbf{x})$:

$$f(\mathbf{x}_{k+1}) \leq f(\mathbf{x}_k) + \alpha\lambda \nabla f(\mathbf{x}_k)^T \delta\mathbf{x}, \quad 0 < \alpha < 1 \tag{32}$$

$$\|\lambda \mathbf{D}_X \delta\mathbf{x}\|_2 > \eta \tag{33}$$

where $f(\mathbf{x}_k)$ is the objective function defined as:

$$f(\mathbf{x}) = \frac{1}{2}\mathbf{F}(\mathbf{x})^T \mathbf{D}_F{}^2 \mathbf{F}(\mathbf{x}) \tag{34}$$

The first condition, given in (32), requires that the average rate of decrease from $f(\mathbf{x}_k)$ to $f(\mathbf{x}_{k+1})$ be at least some fraction of the initial rate of decrease, α. In practice, a very small value of $\alpha = 10^{-4}$ gives acceptable performance. The second condition constrains a weighted l_2 norm of the scalar length of $\mathbf{x}$ to be greater than some minimum prescribed value, η. In (33) and (34), $\mathbf{D}_X$ and $\mathbf{D}_F$ are weighting matrices for $\mathbf{x}$ and $\mathbf{F}$ respectively.

If a value of $\lambda = 1$ does not satisfy the condition given in (32), the value of lambda is found by modelling the following function:

$$g(\lambda) = f(\mathbf{x}_k + \lambda\, \delta\mathbf{x}) \tag{35}$$

as a quadratic or cubic in λ, which is then minimised to find a suitable value of λ. The derivative of (35) with respect to λ at $\lambda = 0$ is:

$$\begin{aligned} g'(0) &= \nabla f(\mathbf{x}_k)\delta\mathbf{x} \\ &= -\mathbf{F}(\mathbf{x}_k)^T \mathbf{D}_F \mathbf{J}(\mathbf{x}_k)\mathbf{J}(\mathbf{x}_k)^{-1}\mathbf{D}_F\mathbf{F}(\mathbf{x}_k) \\ &= -\mathbf{F}(\mathbf{x}_k)^T \mathbf{D}_F{}^2 \mathbf{F}(\mathbf{x}_k) \end{aligned} \tag{36}$$

Equation (35) is first modelled as a quadratic in λ, using the values of $g(0)$ and $g'(0)$ which were obtained at the previous iteration and $g(1)$ which was obtained when attempting the full Newton-Raphson step ($\lambda = 1$). The quadratic can be found to be at a minimum when:

$$\lambda = -\frac{g'(0)}{2\,[g(1) - g(0) - g'(0)]} \tag{37}$$

If the condition described by (32) have not been met, the second and subsequent backtracks model (35) as a cubic in λ. Using the most recent value, λ_1, and the next most recent value, λ_2, the minimum of the cubic can be found to be:

$$\lambda = \frac{-b + \sqrt{b^2 - 3ag'(0)}}{3a} \tag{38}$$

where the parameters, a and b are:

$$\begin{bmatrix} a \\ b \end{bmatrix} = \frac{1}{\lambda_1 - \lambda_2} \begin{bmatrix} \frac{1}{\lambda_1{}^2} & \frac{-1}{\lambda_2{}^2} \\ \frac{-\lambda_2}{\lambda_1{}^2} & \frac{\lambda_1}{\lambda_2{}^2} \end{bmatrix} \begin{bmatrix} g(\lambda_1) - g'(0)\lambda_1 - g(0) \\ g(\lambda_2) - g'(0)\lambda_2 - g(0) \end{bmatrix} \tag{39}$$

At each backtrack, the following additional restriction on lambda, prescribed by [8] is applied:

$$\lambda_1 \;\epsilon\; \left[\frac{\lambda_2}{10},\; \frac{\lambda_2}{2}\right] \tag{40}$$

This process is repeated until either (32) is satisfied, or (33) is violated. In the latter case, a local minimum has been found and the only solution is to start the algorithm from a different initial vector.

A formal description of the algorithm is contained in [11, Appendix E].

D. Globalising the search for the unknown antenna parameters

The problem of finding the antenna parameters from measured $\mathbf{H}$ magnitude and direction at known points is, in the general case, a global minimisation problem, where the global solution to (34) is to be sought. An exact solution for (28) is a specific case that arises in theory, when measurements of the coordinates of the observer points and the magnitude and direction of $\mathbf{H}$ are exact.

In practice, when the system is over specified (more than two observer points) and the measurements used to generate (28) are subject to noise, it ceases to have an exact root. In this general case, a global minimum of (34) still exists, which is in the vicinity of the true solution and is the most likely solution. As the measurement noise becomes excessive, however, this minimum may cease to be the global minimum, leading one to believe that it is not the most likely solution. Intuitively, the likelihood of this happening increases as the noise level increases and decreases as the number of observer points, N, increases.

Given an appropriate initial vector, the algorithm described in III-C is able to solve both the specific and the general cases. This arises because the algorithm is a combination of the Newton-Raphson method and a minimisation method and is able to find both an exact solution to (28), in the theoretical case where it exists (thereby also finding a global minimum to (34)), and a minimum of (34), in the general case.

Although various contemporary algorithms for globalising the solution of (28) were attempted and are described in [11, Appendix F], the most successful of these was a brute-force approach, known in the field of mathematical minimisation as "iterated hill-climbing".

The approach is implemented by simply selecting a number, M, of random initial vectors within the quasi-static region[5], recording the minimum found for each initial vector. Once M solution attempts have been completed, the algorithm removes any duplicate minima found and reports a list of most likely

[5]The values of θ_d, ϕ_d and dipole moment are limited to [0, π], [$-\pi$, π] and a sensible value respectively.

solutions, listed according to their value of $f(\mathbf{x})$. The most likely solution is the one having the least value of $f(\mathbf{x})$.

On an overall level, this algorithm exhibits the most consistent and reliable performance. Another advantage is the insight it offers into the structure of $f(\mathbf{x})$ over the problem space. In the presence of excessive measurement noise, where the solution having the lowest value of $f(\mathbf{x})$ is not necessarily the correct one, the ability to report a list of the most likely solutions found is advantageous.

The algorithm is formally described in [11, Appendix E].

IV. Simulation and testing

A. Simulation methodology

In order to gauge its performance, the algorithm given in section III was simulated using the following general methodology:

1) The quasi-static region was assumed to exist for x, y and z in the interval $[-1000; 1000]$.
2) The magnetic dipole was assigned a random location within the quasi-static region, a random orientation and a random dipole moment, chosen uniformly over the interval $[0; 1]$.
3) A number of observer points, N, were randomly chosen over the quasi-static region.
4) The magnetic field at each observer point was calculated by a field generation routine.
5) The field values and positions of the observer points were input to the algorithm and the solution recorded.
6) The solution was then compared to the original values of dipole position orientation and moment to determine its degree of "correctness".

B. Probability model of the algorithm

The probability of the algorithm yielding a correct solution was experimentally found to have the following cumulative compound distribution function:

$$P(K \leq k) = \int_0^\infty g(x) \left(1 - \left(1 - \frac{1}{x+1}\right)^k\right) dx; \quad k = 1, 2, \ldots \tag{41}$$

where k is the trial number, K is the index of the trial at which the first success occurs, p_k is the probability of success on the kth trial, x is the average number of trials required for success for a given configuration of dipole antenna and observer points and $g(x)$ is the gamma distributed probability density function of x, given by:

$$g(x) = x^{c-1} \frac{e^{-\frac{x}{b}}}{\Gamma(c) b^c}; \qquad 0 \leq x \leq \infty \tag{42}$$

with scale parameter b and shape parameter c.

The distribution described by (41) allows the determination of the number of runs required for the algorithm as a function of the number of observer points in order to obtain a correct solution with a certain confidence. Figure 4 plots the number of trials, k, required versus the numbers of observer points for a range of confidence values.

A detailed description of the probabilistic modelling of the algorithm is described in [11, Appendix G].

C. Simulation of the algorithms using measurements subject to noise

The performance of the algorithm when subject to measurement noise was determined by a adding varying degrees of random noise to the magnetic field magnitude and direction measurements. The $|\mathbf{H}|$ values were corrupted by noise that was randomly distributed to a maximum of 15% of $|\mathbf{H}|$. The angles giving the direction of $\mathbf{H}$ were subject to noise randomly distributed to a maximum of 15% of 360° (54°).

The errors in position, orientation and dipole moment were calculated using the following formulas:

$$R_e = \frac{\sqrt{(x_d - \hat{x_d})^2 + (y_d - \hat{y_d})^2 + (z_d - \hat{z_d})^2}}{\frac{1}{N}\sum_{i=0}^{N} \sqrt{(x_d - x_i)^2 + (y_d - y_i)^2 + (z_d - z_i)^2}} \tag{43}$$

$$\tau_e = \arccos\left(1 - \frac{(\vartheta)^2 + (\varphi)^2 + (\varpi)^2}{2}\right) \tag{44}$$

$$\begin{aligned} \text{where} \quad \vartheta &= \cos(\theta_d) - \cos(\hat{\theta_d}) \\ \varphi &= \sin(\theta_d)\cos(\phi_d) - \sin(\hat{\theta_d})\cos(\hat{\phi_d}) \\ \varpi &= \sin(\theta_d)\sin(\phi_d) - \sin(\hat{\theta_d})\sin(\hat{\phi_d}) \end{aligned}$$

$$NIA_e = \frac{\widehat{NIA}}{NIA} - 1 \tag{45}$$

In (43), (44) and (45), $[\hat{x_d}, \hat{y_d}, \hat{z_d}, \hat{\theta_d}, \hat{\phi_d}, \widehat{NIA}]$ are the calculations of position, orientation and dipole moment based on the noisy measurements. The actual values are given by $[x_d, y_d, z_d, \theta_d, \phi_d, NIA]$.

The error in position is given by (43), which gives the ratio of the distance between actual and calculated values to the mean distance between observer points and actual dipole position. The error in orientation is given by (44), which is derived from the cosine rule and gives the absolute angle by which the calculated orientation differs from the actual orientation.

Figure 5 shows the a linear approximation to the median error in dipole position, orientation and moment for antenna configurations with three, five and ten observer points for additive noise to the magnitude and direction of the magnetic field. Figure 6 shows the error in dipole position and orientation when the dipole moment is known. The median error is used as opposed to the mean error because of its insensitivity to outlying points.

As shown in Figs. 5 and 6, the errors in predicted dipole position, orientation and dipole moment can be dramatically reduced by using five or more observer points.

Actual simulated results, from which the relations in Figs. 5 and 6 are derived, are shown in [11, Appendix H].

D. Field testing of the algorithm

The performance of the algorithm was verified by field testing. A small transmitting loop antenna was used to closely approximate the magnetic dipole source. The antenna was made up of 24 turns of copper wire wound around a circular air core of diameter 20cm. The loop had an inductance of $L = 217\mu$H and, operating at a frequency of 12.8kHz, had a current of $I_{RMS} = 0.4$A flowing through it. The applied dipole moment was therefore $NIA = 0.31\text{Am}^2$.

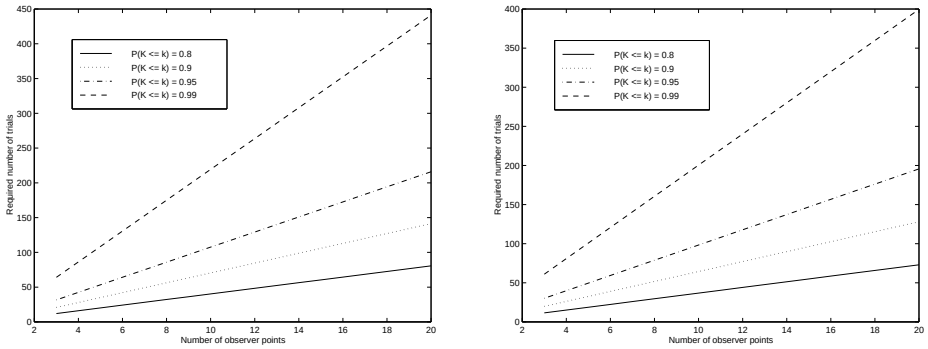

(a) Unknown Dipole Moment. (b) Known Dipole Moment.

Fig. 4. The number of trials required for a correct solution to be found to a certain confidence for varying numbers of observer points .

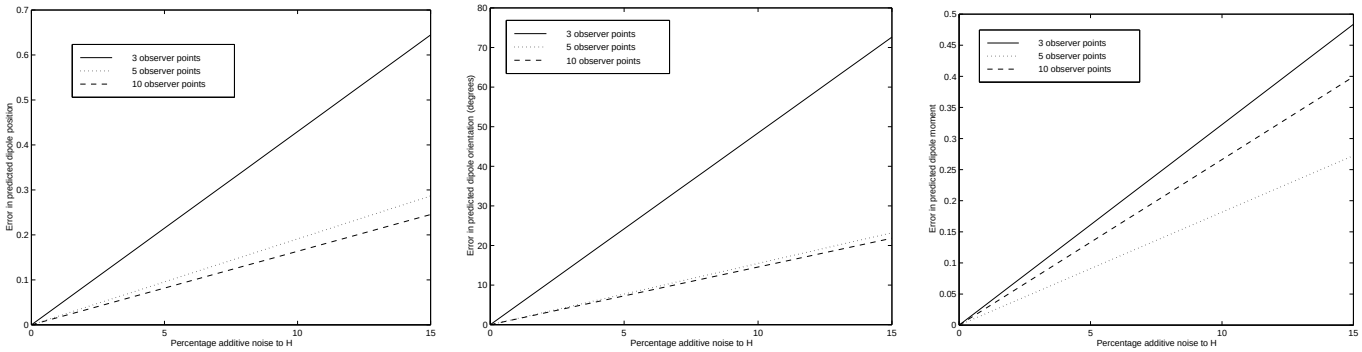

(a) Position. (b) Orientation. (c) Dipole moment.

Fig. 5. The error in predicted position, orientation and dipole moment for increasing values of measurement noise (dipole moment unknown).

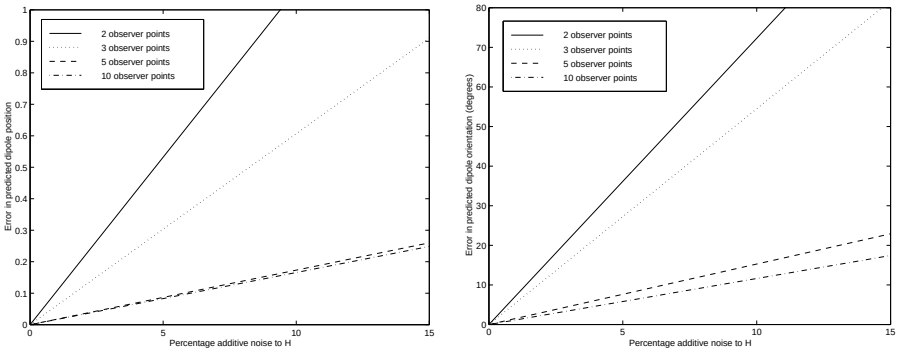

(a) Position. (b) Orientation.

Fig. 6. The error in predicted position and orientation for increasing values of measurement noise (dipole moment known).

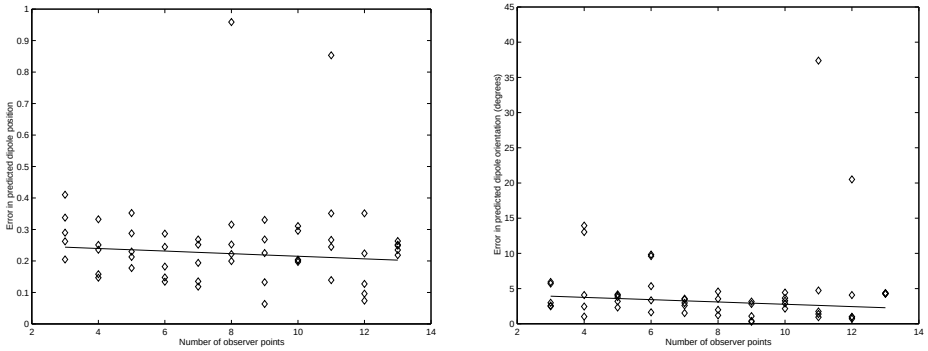

(a) Position. (b) Orientation.

Fig. 7. The error in position and orientation between predicted and known values during field testing for random combinations of up to 13 observer points.

The magnetic field was measured using a receiving antenna system consisting of three orthogonal ferrite loop antennas of 200 turns, wound on 12.5mm diameter ferrite rods, each with an effective relative permeability of $\mu_r = 30$. The antennas were resonated at the operating frequency with a quality factor of $Q = 13$. The magnetic field magnitude was found by taking the vector sum of the voltages induced in the three loops. The direction of the magnetic field was found by taking the ratios of the induced phased voltages.

The test site was a playing field with a stepped concrete grandstand on one side. The dipole was thus located on the surface of a uniform half-space, with the ground beneath it having an estimated conductivity of $\sigma = 10^{-3}\mho\mathrm{m}^{-1}$ and an estimated relative electric permittivity of $\epsilon_r = 20$. The boundary of the quasi-static region in this environment is given by (11) to be $r \approx 100\mathrm{m}$.

With the receiving system positioned at the origin of an assumed coordinate system, the transmitting loop was situated at 13 arbitrarily located points of reception ranging between 5m to 12m from the receiver. The side of the grandstand was used to achieve a variation in height. Using the coordinates of each of the transmitter positions, an equivalent system of observer points for the loop at the origin of the coordinate system was determined.

By comparing the measured values of magnitude and direction of the magnetic field to the predicted theoretical values, an average error of 10% was observed in magnitude and 5° in direction. The error in the coordinates of the observer points was unknown.

Figure 7 shows the results of the test for various random combinations of observer points. The algorithm predicted position and orientation of the transmitting dipole antenna with an average error in position and orientation of 26% and 5° respectively.

V. Conclusion and recommendations for further work

A modified Newton-Raphson algorithm that is able to resolve the unknown position, orientation and dipole moment of a transmitting antenna buried in rock has been presented. Fundamental to the success of the algorithm is the existence of a quasi-static region at a reasonable frequency within the conductive rock. Within this region, the inhomogeneities and anisotropic effects associated with EM wave propagation through rock are negligible, yielding a region in which practical field quantities closely follow theoretical values.

An "iterated hill-climbing" approach can be employed to "globalise" the algorithm. This was shown to be robust with regard to system configuration, yielding predictable and accurate results for a wide range of observer points. One disadvantage of the iterated hill-climbing approach, however, is that it is computationally intensive for systems with a large number of observer points owing to repetitive, continuous inversion of large Jacobian matrices.

The probability of the algorithm yielding a correct solution was found to follow a compound geometric-gamma distribution. The number of runs for a particular likelihood of solution was also shown to be linear with the number of observer points making up the system.

The algorithm proves to be fairly robust with regards to measurement noise. A large improvement in the values of position, orientation and dipole moment may be obtained by using five or more observer points. As expected, in some cases measurement noise causes an incorrect, although mathematically the most likely, solution to be reported.

Field tests of the algorithm yield good results. For an average measurement error of 10% in magnetic field magnitude and 5° in direction, average errors in predicted position and orientation were 26% and 5° respectively.

Recommendations for further work in this field include the following:

- In cases where the number of observer points overspecifies the system of nonlinear equations and the measurements of magnetic field are subject to noise, the least squares solution is found which minimises the error in each equation of (28) equally. Since each observer point yields three equations in (28), a more correct solution may be obtained by weighting each of these three equations differently. This may yield more accurate resolution of position at the expense of accuracy in orientation and dipole moment. Another improvement to the algorithm may be to weight the contribution of each observer point to the solution according to the strength of received magnetic field, since, in practice, the lower the received signal level, the greater its component of noise. More information on the choice of the weighting values and their correlation to *a priori* variance and covariance values may be found in [7].
- It may be known that certain values of the unknown position, orientation and dipole moment of the transmitting antenna are physically unrealisable. In cases such as these, it may be advantageous to constrain the values of the unknowns to be within a particular known range. This involves "penalising" the minimisation function for a value outside the known range. This is a form of nonlinear weighting for the unknowns.
- Finally, the author is of the opinion that the field of adaptive, real-time parameter estimation could lend some additional insight into this problem. Instead of relying on a number of fixed observer points, the field magnitude and direction as well as the real-time position and orientation of a mobile field probe could be input into an algorithm to estimate the unknown antenna parameters using a techniques such as Kalman filtering.

References

[1] A. M. Sommerfeld, "The propagation of waves in wireless telegraphy," *Ann. Phys.*. Ser. 4, Vol. 28, pp. 635–745, 1909.

[2] T. L. Wadley, "Radio Communication through rock on the Wiwatersrand Mines," *CSIR Telecommunications Research Laboratory Report*. ETR-4, 1949.

[3] J. R. Wait, "The magnetic dipole over the horizontally stratified earth," *Canadian Journal of Physics*, Vol. 29, pp. 577–592, 1951.

[4] J. R. Wait, *Electromagnetic Waves in Stratified Media*, Pergamon Press, 1962.

[5] M. N. Kraichman, *Handbook of Electromagnetic Propagation in Conducting Media*, Washington DC, GPO, 1970.

[6] R. Gabillard, P. Degauque and J. R. Wait, "Subsurface Electromagnetic Telecommunication – A Review," *IEEE Transactions on Communications Technology*, Vol. 19, pp. 1217–1228, 1971.

[7] J. R. Wait, "Electromagnetic Induction Technique for Locating a Buried Source," *IEEE Transactions on Geoscience Electronics*, Vol. 9, pp. 95–98, 1971.

[8] J. A. Powell, "An Electromagnetic System for Detecting and Locating Trapped Miners," *US Bureau of Mines, Report of Investigations 8159*, 1976.

[9] N. H. Nessler, "Position finding in mines with ELF waves for arbitrarily oriented transmitters," *Proceedings of the 5th IMEKO Symposium on Intelligent Measurement*. Vol. 1, pp. 232–235, Jena, 1986.

[10] N. H. Nessler, “Location technique with self-locating sensing antennae,” *Measurement*. Vol. 7, No. 1, pp. 13–18, Jan-Mar, 1989.
[11] R. M. Lishman, *An Algorithm for the Automatic Resolution of the Position, Orientation and Dipole Moment of a Magnetic Dipole Antenna Buried in Rock*, MSc Research Report, University of the Witwatersrand, Johannesburg, 2004.
[12] D. R. Vogt, *The Modelling and Design of Radio Tomography Antennas*, PhD dissertation, University of York, 2000.
[13] J. E. Dennis and R. B. Schnabel, *Numerical Methods for Uncontrained Optimization and Nonlinear Equations*, Prentice Hall, 1983.
[14] W. H. Press, S. A. Teukolsky, W. T. Vetterling and B. P. Flannery, *Numerical Recipes in C, The Art of Scientific Computing*, Second Edition, Cambridge University Press, 1992.

APPENDIX A:
DERIVATION OF THE $\mathbf{E}$ AND $\mathbf{H}$ FIELDS FOR AN ELECTRICALLY SMALL LOOP ANTENNA

One of the easiest ways to obtain expressions for the $\mathbf{E}$ and $\mathbf{H}$ fields by developing an expression for the fictitious magnetic vector potential function, $\mathbf{A}$, and then applying widely used expressions that describe $\mathbf{E}$ and $\mathbf{H}$ in terms of derivatives of $\mathbf{A}$. Although this theoretically turns a one step problem into a two step problem, $\mathbf{A}$ involves an easier integration step than if $\mathbf{E}$ and $\mathbf{H}$ were integrated directly.

A-1. Describing $\mathbf{E}$ and $\mathbf{H}$ in terms of $\mathbf{A}$ for a conductive medium

Although these descriptions are widely used in contemporary electromagnetics literature, most derivations of the electric and magnetic fields in terms of $\mathbf{A}$ assume a non-conductive medium. Although the form of the solutions are unchanged, the derivations are detailed here for a conductive medium. They follow the same lines as Balanis [1] and Plonsey & Collin [2].

From (B.4), $\mathbf{B}$ can be expressed as the curl of another vector field, $\mathbf{A}$,

$$\mathbf{B} = \nabla \times \mathbf{A} \tag{A.1}$$

since the vector identity $\nabla \cdot \nabla \times \mathbf{A}$ is equal to zero. The vector, $\mathbf{A}$, is termed the magnetic vector potential. Substituting this into (B.1), one can obtain:

$$\nabla \times (\mathbf{E} + j\omega\mathbf{A}) = 0 \tag{A.2}$$

Equation (A.2) indicates that the field, $\mathbf{E} + j\omega\mathbf{A}$, is irrotational (its curl is zero) and can therefore be expressed as the gradient of another scalar field, Φ, in the following manner:

$$\mathbf{E} + j\omega\mathbf{A} = -\nabla\Phi \tag{A.3}$$

The negative sign in A.3 is arbitrary, it could have been omitted, but for physical relevance to Φ, is included. For conductive media, (B.2) can be expressed as:

$$\nabla \times \mathbf{H} = \mathbf{J}_i + \mathbf{J}_c + j\omega\mathbf{D} \tag{A.4}$$

where $\mathbf{J}_i$ represents the electric current density that is "forced" or impressed by virtue of a source and $\mathbf{J}_c$ represents the conduction current density resulting from $\sigma\mathbf{E}$. Substituting (A.3) into (A.4) for $\mathbf{E}$ and (A.1) into (A.4) for $\mathbf{H}$, one obtains:

$$\frac{1}{\mu}\nabla \times \nabla \times \mathbf{A} = \mathbf{J}_i + (\sigma + j\omega\epsilon)(-\nabla\Phi - j\omega\mathbf{A}) \tag{A.5}$$

Using the vector identity, $\nabla \times \nabla \times \mathbf{A} = \nabla\nabla \cdot \mathbf{A} - \nabla^2\mathbf{A}$, (A.5) reduces to:

$$\nabla\nabla \cdot \mathbf{A} - \nabla^2\mathbf{A} = \mu\mathbf{J}_i + \mu(\sigma + j\omega\epsilon)(-\nabla\Phi - j\omega\mathbf{A}) \tag{A.6}$$

According to the Helmholtz theorem, a vector function is completely specified by its curl and divergence. In (A.1), only the curl of $\mathbf{A}$ was defined. Mathematically speaking, the divergence of $\mathbf{A}$ can be arbitrarily defined without affecting its curl. From a physical point of view, however, an arbitrary definition of $\nabla \cdot \mathbf{A}$ could result in (B.3) not being satisfied, which implies that the charge continuity equation is being violated. To avoid this, the divergence of $\mathbf{A}$ is defined as:

$$\nabla \cdot \mathbf{A} = -\mu(\sigma + j\omega\epsilon)\Phi \tag{A.7}$$

This is known as the Lorentz condition. In addition to simplifying (A.6), defining $\nabla \cdot \mathbf{A}$ in this way ensures that (B.3) is also obeyed as well as the charge continuity equation. Substituting (A.7) into (A.6) gives:

$$\nabla^2\mathbf{A} - j\mu\omega(\sigma + j\omega\epsilon)\mathbf{A} = \nabla^2\mathbf{A} - \gamma^2\mathbf{A} = -\mu\mathbf{J}_i \tag{A.8}$$

where γ is given by (B.10). Equation (A.8) is of a similar form to (B.8) and (B.9), causing a similar $e^{-\gamma R}$ term to appear in the solution. It can be shown that (A.8) is satisfied by the following solution:

$$\mathbf{A} = \frac{\mu}{4\pi} \iiint_V \frac{\mathbf{J}(x', y', z')}{R}\, e^{-\gamma R}\, dv' \tag{A.9}$$

$$\text{where} \quad R = \sqrt{(x - x')^2 + (y - y')^2 + (z - z')^2} \tag{A.10}$$

In (A.9), dv' denotes an infinitesimal volume at coordinates (x', y', z'), which contains a source of current density, while the observation point is at (x, y, z) and R is the distance from source to observation point.

Once $\mathbf{A}$ is determined, $\mathbf{H}$ can be found from (A.1), noting that $\mathbf{B} = \mu\mathbf{H}$. The electric field, $\mathbf{E}$, can either be determined by a combination of (A.3) and (A.7) or from (A.4), with $\mathbf{J}_i = 0$.

A-2. Derivation of the $\mathbf{E}$ *and* $\mathbf{H}$ *fields of a small circular loop in a conductive medium*

The electric and magnetic fields of a magnetic dipole in a homogeneous medium of constitutive parameters $\mu = \mu_0$, ϵ and σ are derived in this section. Although a magnetic dipole is a fictitious concept, its fields are analogous to those of the electric dipole. In practice, a magnetic dipole may be implemented using a loop antenna whose diameter is small when compared with the free-space wavelength.

The derivation for the fields of a small loop follows that given by Balanis [3]. A small loop of radius a is located with its center at the origin of a coordinate system and the plane of the loop oriented in the x-y plane, as shown in Fig. 8. The flow of current is assumed to reside in an infinitely thin circular path in the x-y plane, so the volume integration of (A.9) reduces to:

$$\mathbf{A}(x, y, z) = \frac{\mu}{4\pi} \oint_C \mathbf{I}(x', y')\, \frac{e^{-\gamma R}}{R}\, dl' \tag{A.11}$$

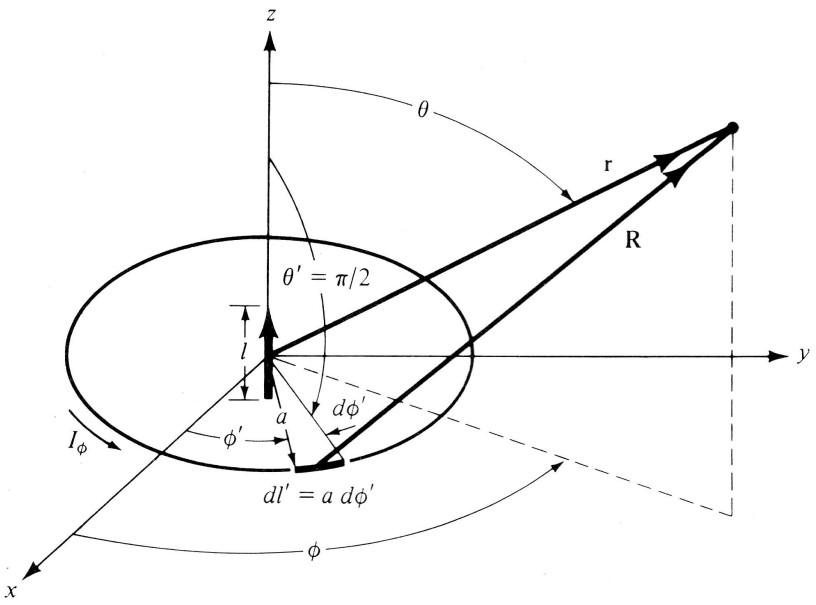

Fig. 8. The configuration of the small circular loop (after [3]).

In (A.11), dl' represents an infinitesimal section of the loop. Since the circumference of the loop is small in comparison to a wavelength, the current flowing in it can be considered to be a constant, I_0. $\mathbf{I}(x', y')$ represents the current vector, given by:

$$\mathbf{I}(x', y') = \hat{\mathbf{a}}_x I_x + \hat{\mathbf{a}}_y I_y \tag{A.12}$$

Since the radiated fields of an antenna are usually easier to express in spherical coordinates, it is desirable to express (A.12) in spherical coordinates. From inspection of Fig. 8, I_x and I_y can be given by:

$$I_x = -I_0 \sin\phi' \tag{A.13}$$

$$I_y = I_0 \cos\phi' \tag{A.14}$$

The rectangular unit vectors, $\hat{\mathbf{a}}_x$ and $\hat{\mathbf{a}}_y$ in (A.12) can be transformed into spherical unit vectors by a rectangular to spherical vector transformation. Equation (A.12) can then be expressed in spherical coordinates as follows:

$$\begin{aligned}\mathbf{I}(\phi') = {} & \hat{\mathbf{a}}_r I_0 \sin\theta \sin(\phi - \phi') + \\ & \hat{\mathbf{a}}_\theta I_0 \cos\theta \sin(\phi - \phi') + \\ & \hat{\mathbf{a}}_\phi I_0 \cos(\phi - \phi')\end{aligned} \tag{A.15}$$

The distance between source and observation points, R, given in (A.10) can also be expressed in spherical coordinates as:

$$R = \sqrt{r^2 + a^2 - 2ar \sin\theta \cos(\phi - \phi')} \tag{A.16}$$

and the infinitesimal length, dl', can be expressed in spherical coordinates as $a\ d\phi'$. A spherical equivalent of (A.11) can then be written as:

$$\mathbf{A}(r,\theta,\phi) = \frac{a\mu}{4\pi}\oint_C \mathbf{I}(\phi')\,\frac{e^{-\gamma R}}{R}\,d\phi'$$
$$= \frac{a\mu I_0}{4\pi}\Bigg[\hat{\mathbf{a}}_r \sin\theta \int_0^{2\pi} \sin(\phi-\phi')f(\phi')\,d\phi' +$$
$$\hat{\mathbf{a}}_\theta \cos\theta \int_0^{2\pi} \sin(\phi-\phi')f(\phi')\,d\phi' +$$
$$\hat{\mathbf{a}}_\phi \int_0^{2\pi} \cos(\phi-\phi')f(\phi')\,d\phi'\Bigg] \tag{A.17}$$

$$\text{where} \quad f(\phi') = \frac{e^{-\gamma\sqrt{r^2+a^2-2ar\sin\theta\cos(\phi-\phi')}}}{\sqrt{r^2+a^2-2ar\sin\theta\cos(\phi-\phi')}} \tag{A.18}$$

Since the loop is symmetrical around the z-axis, the resulting vector potential, $\mathbf{A}$, will not be a function of observation angle, ϕ. Thus, an arbitrary value of $\phi = 0$ is chosen.

The integration of (A.17) cannot be carried out without some approximations. Since a is assumed to be small, $f(\phi')$ can be expanded into a Maclaurin series in a, which, for the first two terms, yields:

$$f(\phi') = f(0) + f'(0)a + \cdots + \frac{1}{(n-1)!}f^{(n-1)}(0)a^{n-1} + \ldots$$
$$\approx \frac{e^{-\gamma r}}{r} + \frac{a\sin\theta\cos\phi'}{r^2}\Big[\gamma r + 1\Big]e^{-\gamma r} \tag{A.19}$$

Using this approximation for $f(\phi')$, (A.17) can be integrated to yield:

$$\mathbf{A} = \hat{\mathbf{a}}_\phi \frac{a^2\mu I_0 \sin\theta}{4r^2}\Big[\gamma r + 1\Big]e^{-\gamma r} \tag{A.20}$$

The magnetic field, $\mathbf{H}$, can then be found to be:

$$\mathbf{H} = \frac{1}{\mu}\nabla\times\mathbf{A}$$
$$= \hat{\mathbf{a}}_r \frac{a^2 I_0\cos\theta}{2r^3}\Big[\gamma r + 1\Big]e^{-\gamma r} +$$
$$\hat{\mathbf{a}}_\theta \frac{a^2 I_0\sin\theta}{4r^3}\Big[(\gamma r)^2 + \gamma r + 1\Big]e^{-\gamma r} \tag{A.21}$$

The electric field, $\mathbf{E}$, is given by:

$$\mathbf{E} = \frac{\nabla(\nabla\cdot\mathbf{A})}{\mu(\sigma + j\omega\epsilon)} - j\omega\mathbf{A}$$
$$= \hat{\mathbf{a}}_\phi \frac{j\omega\mu a^2 I_0\sin\theta}{2r^2}\Big[\gamma r + 1\Big]e^{-\gamma r} \tag{A.22}$$

APPENDIX B:
EM WAVE PROPAGATION IN ROCK

Maxwell's equations in time harmonic form are listed below for convenience. It should be noted that all of **E**, **H**, **D**, **J**, **B** and q represent time harmonic quantities in phasor form. They may thus be complex and are understood to be multiplied by $e^{j\omega t}$. The boldface letters represent vector quantities.

$$\nabla \times \mathbf{E} = -j\omega\mathbf{B} \tag{B.1}$$

$$\nabla \times \mathbf{H} = \mathbf{J} + j\omega\mathbf{D} \tag{B.2}$$

$$\nabla \cdot \mathbf{D} = q \tag{B.3}$$

$$\nabla \cdot \mathbf{B} = 0 \tag{B.4}$$

where $\mathbf{E}$ = vector electric field
$\mathbf{H}$ = vector magnetic field
$\mathbf{D}$ = vector electric flux density
$\mathbf{B}$ = vector magnetic flux density
$\mathbf{J}$ = vector electric current density
q = electric charge density

The constitutive relations allow the uncoupling of Maxwell's equations. They are as follows:

$$\mathbf{D} = \epsilon\mathbf{E} \tag{B.5}$$

$$\mathbf{B} = \mu\mathbf{H} \tag{B.6}$$

$$\mathbf{J} = \sigma\mathbf{E} \tag{B.7}$$

where $\epsilon = \epsilon_r\epsilon_0$ = electric permittivity
$\mu = \mu_r\mu_0$ = magnetic permeability
σ = electric conductivity
ϵ_r = relative permittivity
$\epsilon_0 = 4\pi \times 10^{-7}$ = permittivity of free space
μ_r = relative permeability
$\mu_0 = 8.854 \times 10^{-12}$ = permeability of free space

Maxwell's equations describe and relate the electric and magnetic fields, currents and charge densities at any point in space and time within a medium characterised by the constitutive parameters μ, ϵ and σ. These parameters (μ, ϵ and σ) form the well-known constitutive relations relating magnetic flux density to magnetic field intensity, and electric flux density and electric conduction current density to electric field intensity respectively. The constitutive relations allow the uncoupling of

Maxwell's curl equations to form the following vector wave equations for a region in space that is free from sources:

$$\nabla^2\mathbf{E} = j\omega\mu\sigma\mathbf{E} - \omega^2\mu\epsilon\mathbf{E} = \gamma^2\mathbf{E} \tag{B.8}$$

$$\nabla^2\mathbf{H} = j\omega\mu\sigma\mathbf{H} - \omega^2\mu\epsilon\mathbf{H} = \gamma^2\mathbf{H} \tag{B.9}$$

$$\gamma^2 = j\omega\mu\sigma - \omega^2\mu\epsilon \tag{B.10}$$

In (B.10), γ is termed the propagation constant and consists of a real attenuation component and an imaginary phase component as follows:

$$\gamma = \alpha + j\beta \tag{B.11}$$

where $\alpha =$ attenuation constant (Np/m)
$\beta =$ phase constant (rad/m)

In a region which is unbounded, only traveling waves occur and solutions to (B.8) and (B.9) in a rectangular coordinate system take the following form:

$$\mathbf{E} = \mathbf{f}(x)\cdot\mathbf{g}(y)\cdot\mathbf{h}(z) \tag{B.12}$$

where
$$\mathbf{f}(x) = \mathbf{A}_f\, e^{-\gamma_x x} + \mathbf{B}_f\, e^{+\gamma_x x} \tag{B.13}$$

$$\mathbf{g}(y) = \mathbf{A}_g\, e^{-\gamma_y y} + \mathbf{B}_g\, e^{+\gamma_y y} \tag{B.14}$$

$$\mathbf{h}(z) = \mathbf{A}_h\, e^{-\gamma_z z} + \mathbf{B}_h\, e^{+\gamma_z z} \tag{B.15}$$

$$\gamma^2 = {\gamma_x}^2 + {\gamma_y}^2 + {\gamma_z}^2 \tag{B.16}$$

The terms in $e^{-\gamma_x x}$, $e^{-\gamma_y y}$ and $e^{-\gamma_z z}$ in (B.13), (B.14) and (B.15) represent traveling waves in the $+x$, $+y$ and $+z$ directions respectively. This originates from a positive phase constant, $\beta_{x,y,z}$ in each of those terms. The waves also decay in their respective directions of travel, originating from a positive attenuation constant, $\alpha_{x,y,z}$ in each of the terms. While negative values of $\alpha_{x,y,z}$ and $\beta_{x,y,z}$ also form valid solutions, these are physically meaningless.

In a similar manner, the terms in $e^{+\gamma_x x}$, $e^{+\gamma_y y}$ and $e^{+\gamma_z z}$ in (B.13), (B.14) and (B.15) represent traveling waves in the $-x$, $-y$ and $-z$ directions respectively, again originating from positive phase and attenuation constants. The waves also decay in their respective directions of travel.

Expressions for the attenuation and phase constants in terms of the constitutive parameters of the medium can be found by squaring both sides of (5), substituting the result into (B.10), equating real and imaginary parts and solving for α and β. This gives the following expressions for attenuation and phase constant, also listed in II:

$$\alpha = \omega\sqrt{\mu\epsilon}\left\{\frac{1}{2}\left[\sqrt{1+\left\{\frac{\sigma}{\omega\epsilon}\right\}^2} - 1\right]\right\}^{\frac{1}{2}} \tag{B.17}$$

$$\beta = \omega\sqrt{\mu\epsilon}\left\{\frac{1}{2}\left[\sqrt{1+\left\{\frac{\sigma}{\omega\epsilon}\right\}^2} + 1\right]\right\}^{\frac{1}{2}} \tag{B.18}$$

A conductive medium through which EM waves must travel is frequently characterised by a parameter called the "skin depth". This value gives an idea of the ability of EM waves to penetrate

a conductive medium. More precisely, the skin depth is the distance an EM wave must travel in a conductive medium to attenuate its value to $e^{-1} = 36.8\%$ of the original value. The skin depth in m is given by:

$$\delta = \frac{1}{\alpha} = \frac{1}{\omega\sqrt{\mu\epsilon}\left\{\frac{1}{2}\left[\sqrt{1+\left\{\frac{\sigma}{\omega\epsilon}\right\}^2}-1\right]\right\}^{\frac{1}{2}}} \tag{B.19}$$

The skin depth gives a good indication of the ability of a EM wave to penetrate a particular medium. The presence of the frequency term in the denominator of (B.19) indicates that the lower the choice of operating frequency for a particular conductive medium, the greater will be it's skin depth and the further waves in that medium will travel.

One may argue that any improvement in signal strength afforded by a greater skin depth are offset by the inefficiency of a transmitting antenna at the frequency required to achieve such a skin depth. This would be especially pronounced in the case of the loop antenna, where the radiation resistance rises as ω^4. While this is true, the increased frequency introduces greater complexities with regard to inhomogeneity and anisotropicity of the rock. This influences the degree of determinism in the location process.

Maxwell's curl equation for $\mathbf{H}$, (B.2), shows that $\mathbf{H}$ arises from two components of current density, the conduction current density, $\mathbf{J}_c$, given by $\sigma\mathbf{E}$, and the displacement current density, $\mathbf{J}_d$, given by $j\omega\epsilon\mathbf{E}$. In media where $\sigma \ll \omega\epsilon$, the displacement current density is much greater than the conduction current density and the medium is termed a "good dielectric". Where $\sigma \gg \omega\epsilon$, the conduction current density dominates and the medium is termed a "good conductor". Where $\sigma \approx \omega\epsilon$, neither component of current density dominates and the medium is termed a quasi-conductor.

Gabillard et al. [4] define the "characteristic frequency" of the medium to be the frequency at which the displacement current density equals the conduction current density. At frequencies below the characteristic frequency, the medium is a good conductor, while at frequencies above the characteristic frequency, the medium is a good dielectric. The characteristic frequency can be expressed as:

$$f_c = \frac{1}{2\pi}\frac{\sigma}{\epsilon} \tag{B.20}$$

In cases where either component dominates, Balanis [1] approximates (6), (7) and (B.19) using the expressions in Table I. These expressions show that, for a good conductor, the skin depth is inversely proportional to the square root of both the frequency of the signal and the conductivity of the medium. For a good dielectric, the skin depth is inversely proportional to the conductivity of the medium and proportional to the square root of the permittivity of the medium. Common rock types fall into both of these categories depending on the frequency of operation selected.

The behaviour of electromagnetic waves in rock is subject to the constitutive parameters of the rock. Although in the ideal case, μ, ϵ and σ are constant, in practice they are subject to variations caused by a number of factors which are briefly detailed below:

- Materials whose constitutive parameters are not dependant on the applied field are linear, otherwise they are nonlinear. Most materials exhibit linear behaviour over a certain range of applied fields.
- Isotropic materials are materials whose constitutive parameters are independent of the direction of applied field. If this is not the case, the materials are termed anisotropic and the constitutive parameters can be represented by a 3×3 tensor matrix that relates each component of flux

TABLE I

APPROXIMATE ATTENUATION CONSTANT, PHASE CONSTANTS AND SKIN DEPTH FOR GOOD CONDUCTORS AND DIELECTRICS

	Good Conductor	*Good Dielectric*
Attenuation constant α	$\sqrt{\frac{\omega\mu\sigma}{2}}$	$\frac{\sigma}{2}\sqrt{\frac{\mu}{\epsilon}}$
Phase constant β	$\sqrt{\frac{\omega\mu\sigma}{2}}$	$\omega\sqrt{\mu\epsilon}$
Skin Depth δ	$\sqrt{\frac{2}{\omega\mu\sigma}}$	$\frac{2}{\sigma}\sqrt{\frac{\epsilon}{\mu}}$

density to the components of applied field. Although infrequent, anisotropic rock types do occur in practice.

- If the constitutive parameters of a material are not dependant upon spatial position, the material is homogeneous, otherwise it is inhomogeneous. Obviously, since the earth consists of a complex geological arrangement of rocks, it is of a heterogeneous nature.
- If the constitutive parameters are dependant upon frequency, the material is dispersive, otherwise it is non-dispersive. Although dispersive rock types influence the choice of operating frequency for the methodology, they play no role in the actual operation of the system at a single frequency.

Almost all non-magnetic rock types have a relative magnetic permeability of about unity and show dispersive characteristics in their conductivities and permittivities. A general trend observed for these rock types by Vogt [5], is that the conductivity increases with increasing frequency, while the permittivity drops with increasing frequency. Vogt quotes the measured constitutive parameters of conductivity and permittivity versus frequency of a number of well known rock types occurring across a broad conductivity scale. The measurements were performed using a capacitive sensor into which a disc of rock of diameter 30mm - 80mm and thickness 4mm was placed. The sensor was connected to a vector impedance meter and the rock parameters measured over the 1MHz to 64MHz range.

In [5], Vogt derives frequency dependant models for rock conductivity and permittivity by fitting a Debye model with multiple relaxation times to his measured data. The Debye relationship with a single relaxation time originates from an attempt to explain the dielectric properties of a polar liquid. Since rocks consist of a combination of various crystals, a Debye model with multiple relaxation times is assumed by Vogt. The model takes the following form:

$$\epsilon(\omega) = \epsilon' - j\epsilon'' = \epsilon_\infty + \frac{\epsilon_{\omega_1}}{1 + j\omega\tau_1} + \frac{\epsilon_{\omega_2}}{1 + j\omega\tau_2} + \dots \tag{B.21}$$

$$\epsilon_e = \epsilon' \tag{B.22}$$

$$\sigma_e = \sigma_0 + \omega\epsilon'' \tag{B.23}$$

where
ϵ_∞ = permittivity as $\omega \to \infty$
ϵ_{ω_n} = permittivity at $\omega = \omega_n$
τ_n = nth relaxation time
ϵ_e = effective permittivity
σ_0 = DC conductivity
σ_e = effective conductivity

Although Vogt's models were derived from measured rock properties in the 1MHz – 64MHz range, extrapolation of the model to frequencies below this range still yields meaningful results. Rock

properties in the 100Hz to 10MHz range, shown in Fig. 9, are based on Vogt's models. As with any model, however, a certain amount of error is inevitable, particularly when extrapolating outside the measured range. This error has no effect on the actual location methodology. It's only influence is on determining the choice of operating frequency and the region in space for which the methodology is valid.

The location algorithm developed in section III is based on a linear, isotropic and homogenous earth where the magnetic permeability is assumed to be approximately equal to μ_0. Linearity can reasonably be assumed for the range of field strengths required in underground communications and location. As shown in section II, the greater degree of complexity introduced by an anisotropic, inhomogeneous earth can be minimised by an appropriately low choice of operating frequency.

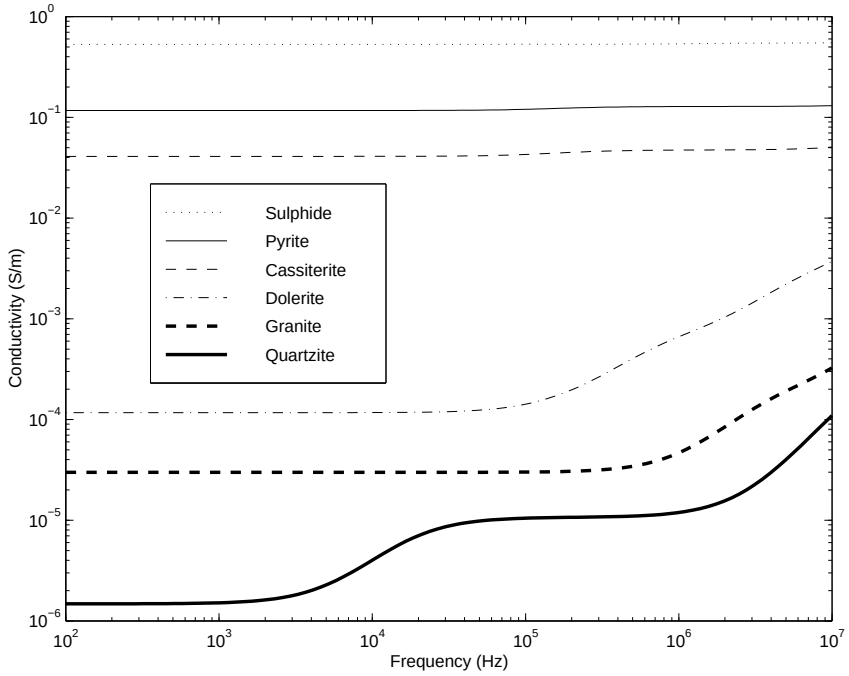

(a) Conductivity.

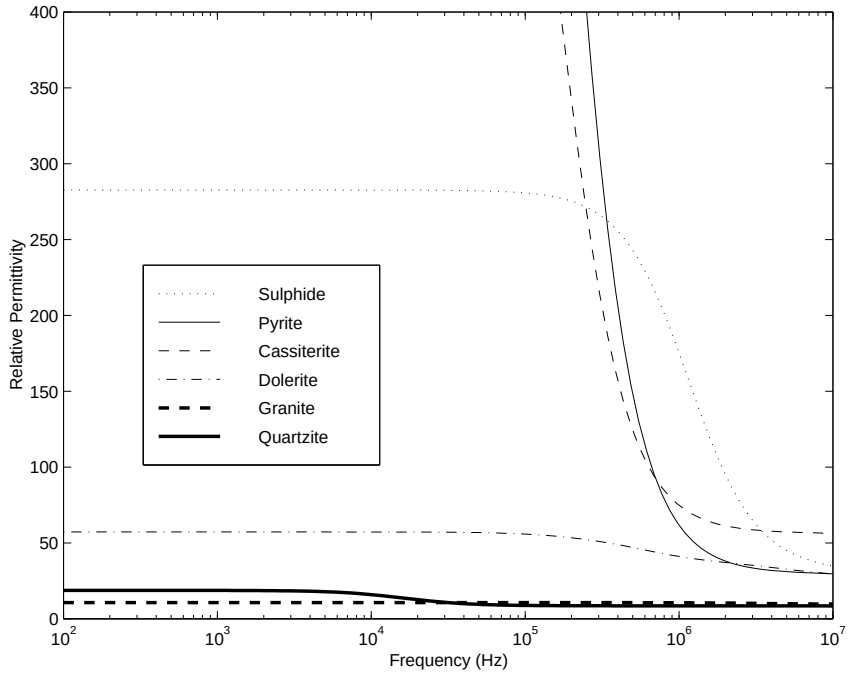

20pt

(b) Relative permittivity.

Fig. 9. The conductivity and relative permittivity of a number of common rock types calculated from Debye models with multiple relaxation times.

APPENDIX C:
A BACKGROUND TO GEOMETRIC TRANSFORMATIONS

Geometric transformations are useful in manipulating geometric objects such as points and vectors. Translation implies moving every point making up the object by an equal distance in a given direction. If $\mathbf{p}$ denotes the point (x, y, z), a translation of p by an amount $\mathbf{t} = (\delta x; \delta y; \delta z)$ is given by:

$$\mathbf{p}^* = \mathbf{p} + \mathbf{t} \tag{C.1}$$

Rotation refers to the rotating a geometric object around an axis in space. The most common form of rotation is rotation around the principal axes. Rotation around the principal axes has three components, namely a rotation β_z around the z-axis, a rotation β_y around the y-axis and a rotation β_x around the x-axis. In a right hand coordinate system, all of β_z, β_y and β_x are positive in an anticlockwise sense when viewed from a point of the $+z$, $+y$ and $+x$-axes, respectively.

Since the magnetic dipole is radially symmetrical about the dipole axis, any orientation of the dipole can be expressed using only two rotations, chosen here to be β_y and β_x. The rotation of a point first around the y-axis and then around the x-axis is given by:

$$\mathbf{p}^* = \mathbf{R}_{yx}\mathbf{p} \tag{C.2}$$

$$\mathbf{R}_{yx} = \begin{bmatrix} \cos\beta_y & 0 & \sin\beta_y \\ \sin\beta_x \sin\beta_y & \cos\beta_x & -\sin\beta_x \cos\beta_y \\ -\cos\beta_x \sin\beta_y & \sin\beta_x & \cos\beta_x \cos\beta_y \end{bmatrix} \tag{C.3}$$

C-1. Derivation of the rotation angles, β_y and β_x, for a given set of spherical angles

Often, the rotation angles β_y and β_x are required to be found for a given set of spherical angles, (θ, ϕ). These can be found by considering the following transformation, also shown in Fig. 10.

Consider a point $\mathbf{p}$, situated on the z-axis, such that its rectangular coordinates are given by $(0, 0, r)$ for some value of r. Since rotation of a point does not change the distance between the origin and the point, any rotation of $\mathbf{p}$ will have a magnitude of r. If $\mathbf{p}$ is rotated, first around the y-axis and then around the x-axis, to arrive at a point $\mathbf{p}^*$, the new rectangular coordinates of $\mathbf{p}^*$ will be given by $(r\sin\theta\cos\phi; r\sin\theta\sin\phi; r\cos\theta)$. Substituting $\mathbf{p}$ and $\mathbf{p}^*$ into (C.2), one obtains:

$$\begin{bmatrix} \sin\theta\cos\phi \\ \sin\theta\sin\phi \\ \cos\theta \end{bmatrix} = \begin{bmatrix} \sin\beta_y \\ -\sin\beta_x\cos\beta_y \\ \cos\beta_x\cos\beta_y \end{bmatrix} \tag{C.4}$$

Expressions for β_y and β_x can then be found to be:

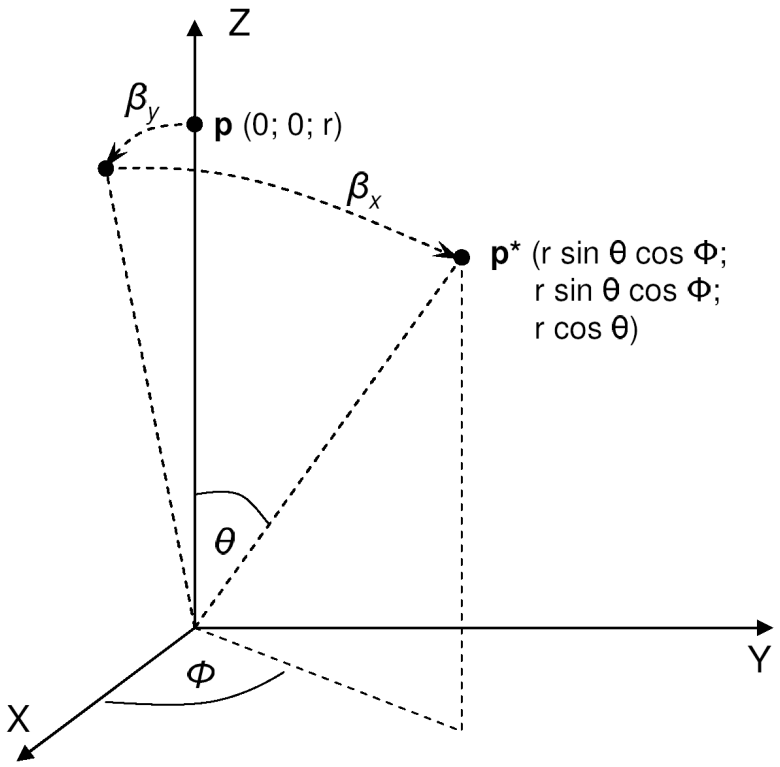

Fig. 10. Finding the rotation angles β_y and β_x for a given set of spherical angles.

$$\begin{bmatrix} \beta_x \\ \beta_y \end{bmatrix} = \begin{bmatrix} \arctan\left(-\dfrac{\sin\theta\sin\phi}{\cos\theta}\right) \\ \arcsin\left(\sin\theta\cos\phi\right) \end{bmatrix} \tag{C.5}$$

C-2. Rotation of spherical angles (θ_1, ϕ_1) *to* (θ_2, ϕ_2)

Another common task is the rotation of a set of spherical angles (θ_1, ϕ_1) first around the y-axis by β_y and then around the x-axis by β_x to arrive at the transformed set of spherical angles, (θ_2, ϕ_2). The transformed spherical angles can be found by the following transformation.

If one considers a point $\mathbf{p}_1$, having spherical coordinates (r, θ_1, ϕ_1), its rectangular coordinates will be given by $(r\sin\theta_1\cos\phi_1; r\sin\theta_1\sin\phi_1; r\cos\theta_1)$. Again, since rotation of a point does not change the distance between the origin and the point, any rotation of $\mathbf{p}_1$ will have the same magnitude, r. If $\mathbf{p}_1$ is rotated, first around the y-axis and then around the x-axis, to arrive at a point $\mathbf{p}_2$, the new rectangular coordinates of $\mathbf{p}_2$ will be given by $(r\sin\theta_2\cos\phi_2; r\sin\theta_2\sin\phi_2; r\cos\theta_2)$. Since $\mathbf{p}_1$ is the original point and $\mathbf{p}_2$ the transformed point, substituting them for $\mathbf{p}$ and $\mathbf{p}^*$ respectively in (C.2) yields:

$$\mathbf{U} = \begin{bmatrix} \sin\theta_2\cos\phi_2 \\ \sin\theta_2\sin\phi_2 \\ \cos\theta_2 \end{bmatrix} = \mathbf{R}_{yx} \begin{bmatrix} \sin\theta_1\cos\phi_1 \\ \sin\theta_1\sin\phi_1 \\ \cos\theta_1 \end{bmatrix} \tag{C.6}$$

$$\theta_2 = \arccos\left(U_3\right) \tag{C.7}$$

$$\phi_2 = \arctan\left(\frac{U_2}{U_1}\right) \tag{C.8}$$

More information relating to geometric transformations can be found in [6].

APPENDIX D:
THE NEWTON-RAPHSON ALGORITHM WITH LINE SEARCHES AND BACKTRACKING

It is worth noting that there are no "good" general methods for solving systems of nonlinear equations. As put by Press et al. [7], *"there never will be any good general methods for solving systems of nonlinear equations"*. Solving a system of nonlinear equations is, in effect, a simultaneous N-dimensional minimisation problem where at each iteration, the system as a whole has to be taken closer to a solution, although possibly at the expense of an individual dimension. The choice as to how much progress in one dimension of the problem space is worth compared to progress in the other dimensions involves many tradeoffs.

The Newton-Raphson method is an iterative method taking the following form:

$$\mathbf{x}_{k+1} = \mathbf{x}_k + \delta\mathbf{x} \tag{D.1}$$

The update term, $\delta\mathbf{x}$ is derived from the expansion of (28) in a Taylor series, which yields:

$$F_i(\mathbf{x} + \delta\mathbf{x}) = F_i(\mathbf{x}) + \sum_{j=1}^{N} \frac{\partial F_i}{\partial x_j}\delta x_j + \dots \tag{D.2}$$

In matrix notation, (D.2) can be written in matrix notation as:

$$\mathbf{F}(\mathbf{x} + \delta\mathbf{x}) = \mathbf{F}(\mathbf{x}) + \mathbf{J} \cdot \delta\mathbf{x} + \dots \tag{D.3}$$

where $\mathbf{J}$ is the Jacobian matrix, given by:

$$\mathbf{J}(\mathbf{x}) = \begin{bmatrix} \frac{\partial F_1}{\partial x_1} & \cdots & \frac{\partial F_1}{\partial x_6} \\ \vdots & \vdots & \ddots \\ \frac{\partial F_N}{\partial x_1} & \cdots & \frac{\partial F_N}{\partial x_6} \end{bmatrix} \tag{D.4}$$

By setting $\mathbf{F}(\mathbf{x} + \delta\mathbf{x}) = 0$ and neglecting higher order terms, the following expression is obtained for δx:

$$\delta\mathbf{x} = -\mathbf{J}(\mathbf{x})^{-1}\mathbf{F}(\mathbf{x}_k) \tag{D.5}$$

Equation (30) is a linear matrix equation that can be solved by *QR* decomposition or singular value decomposition.

Despite the excellent local convergence properties of the Newton-Raphson method, its global convergence ability is poor[6]. Many methods do exist, however, for extending the region of local convergence of the Newton-Raphson method. These include methods that combine gradient-based minimisation methods with the Newton-Raphson method. The Newton-Raphson method with line searches and backtracking uses a Newton-Raphson iteration wherever it makes mathematical sense. Where it does not make mathematical sense, a minimisation step is used instead.

Suppose, after iteration k, $\mathbf{x}_{k+1}$, given by (D.1), was the vector of unknowns. How does one determine whether $\mathbf{x}_{k+1}$ is moving closer to a solution? An intuitive answer is:

$$\|\mathbf{D}_F\mathbf{F}(\mathbf{x}_{k+1})\| < \|\mathbf{D}_F\mathbf{F}(\mathbf{x}_k)\| \tag{D.6}$$

for some norm, where $\mathbf{D}_F$ is a diagonal scaling matrix for $\mathbf{F}$. A convenient norm to choose is the l_2 norm. By requiring that each iteration of $\mathbf{x}$ decrease $\|\mathbf{D}_F\mathbf{F}(\mathbf{x}_{k+1})\|_2$, one can extend this line of reasoning to finding a minimum of $\|\mathbf{D}_F\mathbf{F}(\mathbf{x}_{k+1})\|_2$, defined as:

$$\min_{\mathbf{x}\epsilon\mathbb{R}^n} f(\mathbf{x}) = \frac{1}{2}\mathbf{F}(\mathbf{x})^T{\mathbf{D}_F}^2\mathbf{F}(\mathbf{x}) \tag{D.7}$$

It should be noted that every solution to (28) minimises (D.7), but not every minimum found by (D.7) is a solution to (28), since it could be a local minimum. Thus, one can not simply solve for a local minimum of (D.7) and expect the solution to satisfy (28).

Dennis and Schnabel [8] show that the Newton-Raphson step, given by (30) is a descent direction that can be used to minimise (D.7). One way to combine the two methods is, at each iteration, to first attempt a full Newton-Raphson step. If the step reduces $f(\mathbf{x})$ sufficiently, it is acceptable. If not, one can backtrack along the Newton-Raphson direction and be guaranteed of finding a solution to (D.6), since the Newton-Raphson direction is a descent direction.

For the globally convergent method, the update equation for $\mathbf{x}$ is given by:

$$\mathbf{x}_{k+1} = \mathbf{x}_k + \lambda\delta\mathbf{x}, \qquad 0 < \lambda \leq 1 \tag{D.8}$$

The obvious problem is how to choose λ such that an acceptable iteration is obtained. One option is to find a value of λ such that (D.6) is satisfied. While this is logical, there exist cases where the sequences of iterates satisfy (D.6), but fail to converge. Two criteria that guarantee convergence are given by Dennis and Schnabel [8] to be:

$$f(\mathbf{x}_{k+1}) \leq f(\mathbf{x}_k) + \alpha\lambda\,\nabla f(\mathbf{x}_k)^T\delta\mathbf{x}, \qquad 0 < \alpha < 1 \tag{D.9}$$

$$\nabla f(\mathbf{x}_{k+1})^T\delta\mathbf{x} \geq \beta\,\nabla f(\mathbf{x}_k)^T\delta\mathbf{x}, \qquad \alpha < \beta < 1 \tag{D.10}$$

The first condition is identical to that given in section III-C. The second condition requires that the rate of decrease of f at $\mathbf{x}_{k+1}$ be greater than some fraction of the rate of decrease of f at $\mathbf{x}_k$. In practice, this requirement is generally not needed because of the use of a backtracking strategy. Also, since it requires evaluation of $\mathbf{J}(\mathbf{x}+\lambda\,\delta\mathbf{x})$, the simpler condition given by (33) in section III-C is used instead.

[6]The phrase global convergence implies the ability of the method to find a solution to (28) no matter what starting point in the unknown space is chosen. This is contrast with local convergence, which implies that the solution finding ability is restricted to a region in the unknown space around the solution.

Another option to obtain an acceptable iteration is to choose λ such that (D.7) is minimised exactly, which, until the early 1970s, was the approach taken. As reported by Press et al. [7], this is computationally wasteful, however, and a more computationally efficient but equally effective means of choosing λ is using the method given in section III-C.

While the algorithm described above is more likely to find a solution to (28) where the Newton-Raphson method itself might fail, it is still not a globally convergent algorithm in the sense that it will find a solution regardless of the starting point in the unknown space. The algorithm can encounter a local minimum that it is unable to escape from. This is characterised by multiple backtracks, very small steps and values of $f(\mathbf{x})$ that tend to stagnate as each iteration hunts for a nonexistent root.

APPENDIX E:
A FORMAL DESCRIPTION OF THE LOCATION ALGORITHM

A formal description of the Newton-Raphson algorithm with line searches and backtracking is given as follows:

1) Perform the following until either $\mathbf{x}_k$ has converged to a satisfactory precision, or $f(\mathbf{x})$, given by (D.7), has stagnated, or the maximum number of iterations has been reached.
   a) For each of N observer points, i, do the following:
      i) Determine β_x and β_y from (θ_d, ϕ_d) in $\mathbf{x}_k$ using (22).
      ii) Determine (x_i^*, y_i^*, z_i^*) from (23) using the calculated values of β_x and β_y, the location of the observer point, (x_i, y_i, z_i), and the unknown location of the dipole, (x_d, y_d, z_d) from $\mathbf{x}_k$.
      iii) Determine θ_i^* and ϕ_i^* from (26) and (27) using the calculated values of β_x and β_y, the angle of the magnetic field at the observer point, (θ_i, ϕ_i).
      iv) Form one of the entries of $\mathbf{F}$, F_{3i-2}, by substituting the magnitude of the magnetic field at the observer point $|\mathbf{H}_i|$, (19) and (20) into (15).
      v) Form another of the entries of $\mathbf{F}$, F_{3i-1}, by substituting (27) and (21) into (16).
      vi) Form another of the entries of $\mathbf{F}$, F_{3i}, by substituting (26) and (20) into (18).
      vii) Find the values of $F_{3i-2}(x_j+h)$, $F_{3i-1}(x_j+h)$ and $F_{3i}(x_j+h)$ for all j by perturbing each element x_j of $\mathbf{x}$ in turn by h and recalculating steps (1(a)i) to (1(a)iii).
      viii) For each row of the Jacobian matrix, J_{3i-2}, J_{3i-1} and J_{3i}, the jth element can be formed by substituting $F_{3i-2}(x_j + h)$, $F_{3i-1}(x_j + h)$ and $F_{3i}(x_j + h)$ into (31).
   b) Determine $\delta\mathbf{x}$ using (30).
   c) Determine $g(0)$, $g(1)$ and $g'(0)$ using (35) and (36).
   d) If (32) is not satisfied, perform the following backtracks until it is satisfied, or the step length violates (33).
      i) If this is the first backtrack, use (37) to find λ for the quadratic approximation to $g(\lambda)$. Otherwise, use (38) to find λ for the cubic approximation to $g(\lambda)$.
      ii) Constrain λ according to (40).
      iii) Evaluate the new value of $g(\lambda)$ to determine whether (32) is satisfied.
   e) Update the iterate, $\mathbf{x}_k$, using (29).
   f) Record the current iterate, $\mathbf{x}_k$, in a history log, as well as the value of $f(\mathbf{x}_k)$ for that solution and the number of backtrack operations performed in the current iteration.
2) Report the last iterate solution calculated, $\mathbf{x}_n$, as well as the value of $f(\mathbf{x}_n)$, the number of iterations, n, and the iteration history.

A formal description of the iterated hill-climbing algorithm is as follows.

1) For each of M solution attempts, do the following:
   a) Generate a random initial vector in the problem space, $\mathbf{x}_0$.
   b) Call NRSOLVE, passing $\mathbf{x}_0$ to it.
   c) Record the resulting solution and value of $f(\mathbf{x})$ in a history log.
2) Eliminate duplicate minima and solutions whose iterations expired from the history log.
3) Assign each minima in the history log a probability according to its value of $f(\mathbf{x})$.
4) Report the most likely minima found, in order of their probability.

The algorithms are termed NRSOLVE and IHCSOLVE respectively and are coded in MATLAB and contained in [9] and [10]. The module help files give a description on the format of input and output parameters.

APPENDIX F:
CONTEMPORARY GLOBAL MINIMISATION ALGORITHMS ATTEMPTED IN THE SEARCH FOR THE UNKNOWN ANTENNA PARAMETERS

F-1. Genetic Algorithm

One of the most intriguing global minimisation methods researched was that of using a genetic algorithm. A genetic algorithm is based on the genetic processes of biological organisms and exhibits characteristics such as "natural selection" and "survival of the fittest". A genetic algorithm can be thought of as a guided random search method that improves on the random search described in III-D in that it provides the advantage of exploring the problem space in parallel, starting from an undirected search that gets more specific after each generation. A general outline of the method is given below. For a more in depth discussion on the topic of genetic algorithms, interested readers are referred to [11] and [12].

A random "population" of vectors in the problem space is chosen. Each of the members of the population is a candidate for the possible solution to (34) and is evaluated in terms of its fitness. The least fit members are replaced by other random members, while the highly fit members are given an opportunity to breed with the other members of their population to produce offspring. A new population is then formed that consists of the fittest few of the old population, as well as the new offspring. Random mutations are also introduced into the population.

This process is repeated a number of times. Over many generations, characteristics that minimise (34) are spread throughout the population. By favouring the breeding of the more fit members, the most promising areas of the problem space are explored. If the algorithm has been designed well, the population will converge on an optimal solution to the problem, the global minimum of (34).

The issue of breeding is probably the most critical one in any genetic algorithm. This encompasses two activities, mating and crossover. Mating refers to the decision of which members of the population to pair together to produce offspring. Crossover refers to the way in which the characteristics of each parent are combined to produce offspring.

After a number of trial and error attempts, the best results were obtained through the concept of allowing a number of the fittest members of the population to mate with every other member of the population, each "rendezvous" producing a number of offspring. This is in contrast to other implementations of genetic algorithms, where the opportunity to mate that is afforded each member of the population is a direct function of their fitness. Experience showed, however, that this conventional method caused the population to be quickly dominated by one minimum, which was not necessarily the global minimum. In contrast, the unbiased approach to mating that was chosen allowed the population to support more than one concurrent minimum, giving the algorithm a chance to decide over a number of generations which minimum was "more global" than the others.

In order to, as much as possible, prevent the population from getting stuck in a local minimum, new random members are introduced. The elite of the population are allowed to mate with the new members, producing two identical offspring. The benefit of producing two identical offspring is that, should they discover a better minimum than the current one, they are able to breed with each other and allow this promising new area of the problem space to be explored.

Although many methods for crossover exist, the one which gave the most favourable results was a continuous form of crossover. In this form of crossover, a random vector is generated whose entries range continuously between zero and one. Offspring are produced by combining each characteristic of the parents in the ratio specified by the random vector.

At each generation, all the members of the population except an elite few are mutated by a small degree. The purpose of mutation is to provide incrementally small steps by which the solution is able to be improved at each generation. It was found that, in order to further improve the solution as it got progressively closer to the global minimum, one needed to decrease the amount by which the members of the population are mutated. This is logical, considering the fact that as one gets progressively closer to a solution, the amount by which it needs to be improved gets smaller[7].

The genetic algorithm is coded in MATLAB and is contained in [13]. The module help file gives a description on the format of input and output parameters. A formal description of the routine, termed GASOLVE, is as follows:

1) Generate the population by choosing a number of random vectors in the problem space.
2) Do the following until the target fitness of the population has been reached, or L generations have been completed:
   a) Evaluate the fitness of each member of the population by calculating the $\mathbf{F}$ vector using steps (1(a)i) to (1(a)vi) of NRSOLVE and using the formula:

$$\text{fitness} = \frac{1}{4}\sqrt{f(\mathbf{x})} \tag{F.1}$$

   b) Sort the population according to fitness.
   c) Restrict the population size to its original size.
   d) Replace a number of the least fit members of the population by new random members.
   e) Determine the mutation factor from the fittest member of the population according to the following formula:

$$\text{mutation factor} = \left(\frac{9\ \text{fitness}}{N}\right)^{-\frac{3}{2}} \tag{F.2}$$

   f) Form a new population by including the following members:
      i) A number of elite individuals from the population.
      ii) The offspring produced by breeding a number of the fittest members of the population with the rest of the population.
      iii) A pair of identical offspring produced by breeding the elite of the population with the new random members of the population.
   g) According to a certain probability, mutate the attributes of each member by a uniform random amount bounded by the mutation factor calculated in (2e).
3) Report the fittest member of the population, the fitness, and the number of generations run.
4) Polish the result by calling NRSOLVE with the fittest member and reporting the result.

Although the algorithm performs excellently in some cases, especially as the number of observer points increases, given certain antenna and observer point configurations, it converges on a local minimum and gives an incorrect result. This behaviour seems to be highly dependant on the parameters of the problem and cannot be predicted. Another drawback is that one has no idea of the reported solution when compared to other alternative solutions, causing an inability to decide on the viability of the reported solution. The algorithm is, however, computationally efficient when the number of observer points is large.

[7] A good analogy to this is that of a player on a golf course. As the ball gets closer to the pin, the strength with which the player needs to hit it gets smaller.

The simulated performance of the genetic algorithm for differing numbers of observer points and various levels of measurement noise is given in section IV.

F-2. Simulated annealing

Another globalisation method attempted was that based on the principle of "simulated annealing". This is a technique that has its roots in the field of thermodynamics and has enjoyed much success in solving various difficult combinatorial and continuous optimisation problems. Initially, the search for a solution is subject to a great amount of randomness, but as iterations go by, the method slowly decreases this random activity, analogous to cooling its temperature. As the temperature continues to cool, the solution gradually "solidifies", frequently on the global minimum. Its benefit lies in the fact that the algorithm has a chance to escape from local minima, converging on the global minimum over time.

The technique of simulated annealing draws its roots from the thermodynamic analogy of the way in which liquids freeze and crystallise and the way that metals cool and anneal. At high temperatures, the atoms or molecules of the substance are very mobile, but, as the temperature drops off, they become less mobile. An amazing phenomenon is that, if the system is cooled slowly enough, the individual atoms or molecules of the substance are able to align themselves over great distances, typically many million times the dimension of an individual atom. This alignment corresponds to the minimum energy state of the substance. Thus, if cooled sufficiently slowly, the substance is able to "minimise" its energy state. If, on the other had, the substance is cooled quickly, it ends up in a higher energy state. The determining factor of how well the system is able to minimise its energy depends on the rate at which it is cooled, slow cooling allowing ample time for the atoms and molecules to readjust themselves.

Press et al. [7] show how this physical process is related to the Boltzmann probability distribution relating the probability of the energy of the system to its temperature. Even at a low temperature, there is a finite probability, although small, of the system being in a high energy state. So, as the molecules attempt to align themselves to minimise their energy state, there is a finite probability that they will jump to a higher energy state, according to the Boltzmann probability distribution. This has the effect of throwing the system out of local minima. As the temperature of the system decreases, the Boltzmann distribution tends toward the system state that has a lower energy and, if the temperature is sufficiently slow, toward the system state that has the lowest energy, the global minimum.

This principle was first incorporated into numerical calculations by Metropolis et al. [14], who realised that the physical process could be simulated at a particular temperature using Monte Carlo methods to generate a number of system states. This concept has since been used to solve a variety of difficult optimisation problems.

The simulated annealing algorithm used to solve for the unknown antenna parameters is simple. The "energy state" of the system is assumed to be given by $f(\mathbf{x})$ in (D.7). The temperature decay is assumed to be exponential, given by:

$$T = T_0 \, e^{-\frac{t}{\tau}} \tag{F.3}$$

where T_0 is the initial temperature, and τ is the temperature time constant.

For a given temperature, the probability that the system will jump to a state having an energy differential Δf from the current state is assumed to be:

$$p = e^{-\frac{\Delta f}{T}} \tag{F.4}$$

The algorithm starts by choosing a random current vector within the problem space. The energy state is calculated for this vector. At each time iteration, a new random vector is chosen and its energy state calculated. If the new energy state is lower than the current energy state, or if the new energy state is higher than the current and a generated random number falls below (F.4), a different current vector is found by performing one iteration of the modified Newton-Raphson algorithm with the new vector as the initial point. Otherwise, if the new energy state is higher than the current and a generated random number falls above (F.4), then the current vector is updated by performing another iteration of the modified Newton-Raphson algorithm on it.

The algorithm was tested using a variety of different time lengths, temperature time constants and initial temperatures. Although it sometimes arrives at the correct solution, its performance is sporadic at the best of times.

The algorithm is coded in MATLAB and is contained in [15].

APPENDIX G:
PROBABILISTIC MODELLING OF THE ALGORITHM)

In quantifying the practical performance of the modified Newton-Raphson algorithm, some very obvious questions arise.

1) Firstly, what is the likelihood that the algorithm will find a solution?
2) Secondly, how many iterations of the algorithm will be needed to produce a solution with a certain confidence.

For a given configuration of antenna parameters and observer points, the modified Newton-Raphson algorithm will yield one of two possible outcomes for a randomly selected initial vector. Either a global minimum to (34) is found, or a local minimum is found, or, in other words, either the outcome is a "success", or it is a "failure". In the language of statistics, each run of the algorithm is a Bernoulli trial producing one of two outcomes. The number of trials required for one successful outcome is then described by the geometric distribution [16].

The geometric probability density function is given as:

$$p_k = P(K = k) = (1 - q)^{k-1} q; \qquad k = 1, 2, \ldots \tag{G.1}$$

where k is the trial number, K is the index of the trial at which the first success occurs, q is the probability of success on a trial and p_k the probability of success on the kth trial. The probability of success on a trial and the expected value, or mean, of the geometric distribution are reciprocally related. The probability that success has occurred by the kth trial is given by the cumulative distribution function of K, given by:

$$P(K \leq k) = \sum_{i=1}^{k} p_i = 1 - (1 - q)^k; \qquad k = 1, 2, \ldots \tag{G.2}$$

It can be seen that the geometric density and distribution functions are completely specified by q, the probability of success on a trial, or the reciprocal of the mean number of trials between successes.

This distribution was verified in simulation by choosing a random configuration of antenna parameters and observer points and continuously running the algorithm with a randomly chosen initial vector and recording the number of runs between exact solutions. As the number of runs becomes large, the distribution of intervals between successes approaches the geometric distribution. Figure 11 shows an empirical distribution obtained for 10 000 runs of the algorithm, showing a close approximation to the geometric distribution.

As the configuration of antenna parameters and observer points changes, so does the probability of success of a single trial. For a fixed number of observer points, this probability was simulated and its inverse, the average number of trials between successes was found to have a shifted Gamma distribution. The distribution is shifted since it obviously has a lower limit of one, while the gamma distribution has a lower limit of zero.

The probability density function for the Gamma distribution was given by (42) in section IV-B. The scale parameter b and shape parameter c can be found by a method such as maximum likelihood

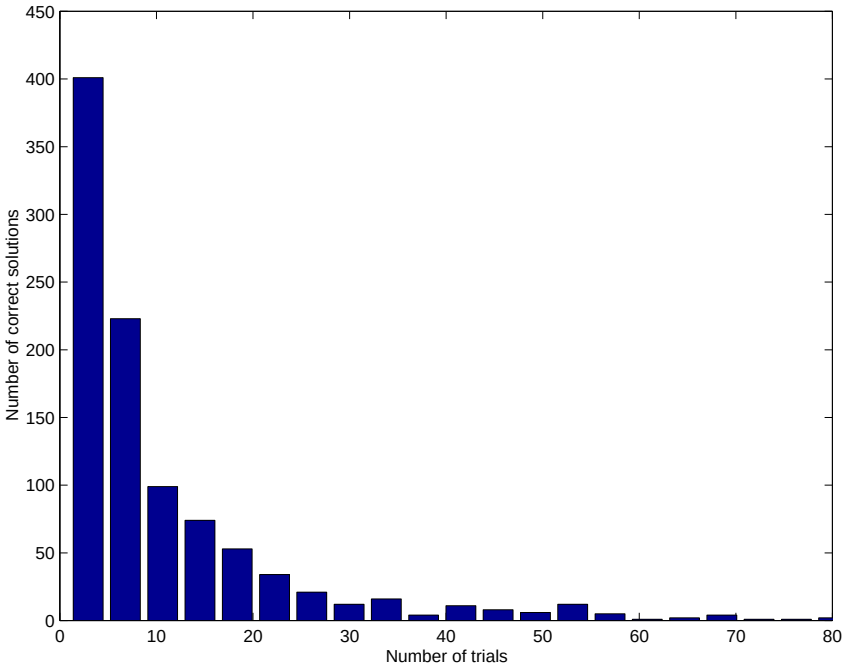

Fig. 11. The distribution of iterations between correct outcomes of the algorithm for one random configuration of antenna parameters and observer points.

estimation.

The overall probability that a solution is found by k intervals, for any configuration is the sum of individual probabilities of the infinite set of gamma distributed means multiplied by the probability that a solution is found within by k intervals for that mean. Using this reasoning, one arrives at the cumulative compound distribution function given in (41) in section IV-B.

The cumulative distribution function was verified using a simulation of 100 000 runs of the algorithm at 100 different antenna configurations. The distribution function values were calculated by numerically integrating (42). The calculated results closely approximate the empirically obtained results, as shown in Fig. 12. A MATLAB routine for numerically calculating the integral in (41) is contained in [17].

The cumulative distribution function allows one to answer the question initially posed in this section by determining a value of k such that the probability of the algorithm finding a solution is greater than a certain probability. This value can then be used as an input to the iterated hill climbing algorithm to give a solution with a certain probability.

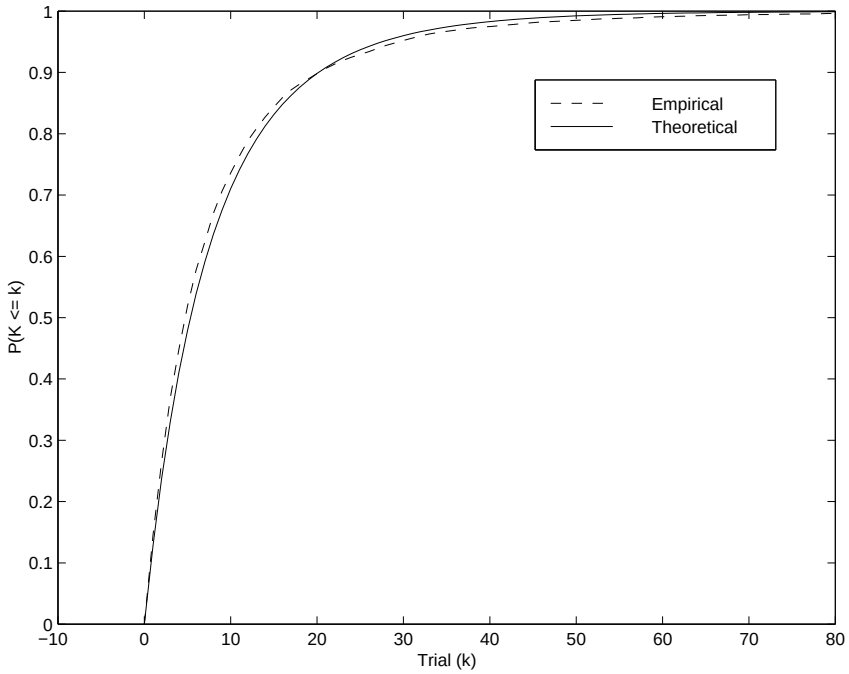

Fig. 12. The empirical and cumulative distributions of the number of trials of the algorithm required for a correct solution for an arbitrary configuration of antenna parameters and observer points.

APPENDIX H:
SIMULATED RESULTS OF THE ALGORITHM USING MEASUREMENTS SUBJECT TO NOISE

This section gives the actual results obtained in the simulation of the algorithm using measurements subject to noise.

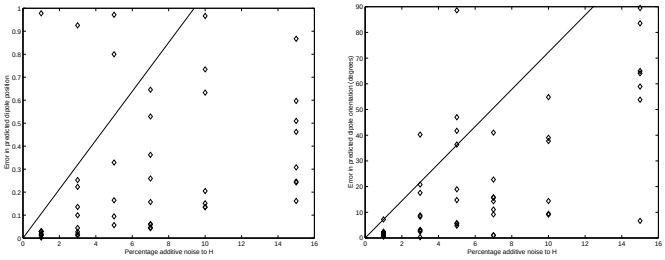

(a) Position. (b) Orientation.

Fig. 13. The error in predicted position and orientation for increasing values of measurement noise (two observer points, dipole moment known).

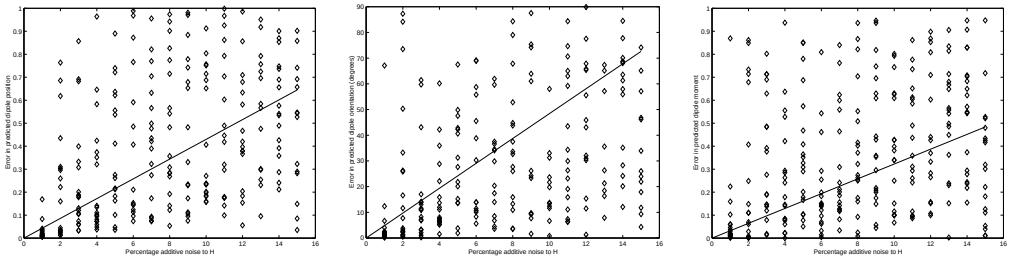

(a) Position. (b) Orientation. (c) Dipole moment.

Fig. 14. The error in predicted position, orientation and dipole moment for increasing values of measurement noise (three observer points, dipole moment unknown).

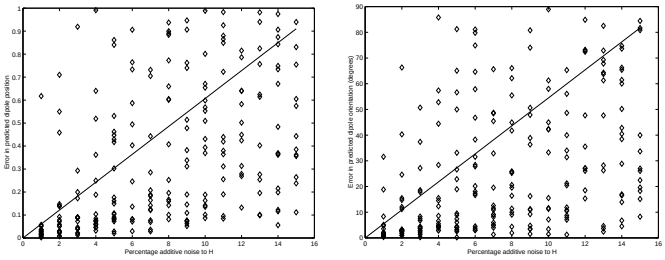

(a) Position. (b) Orientation.

Fig. 15. The error in predicted position and orientation for increasing values of measurement noise (three observer points, dipole moment known).

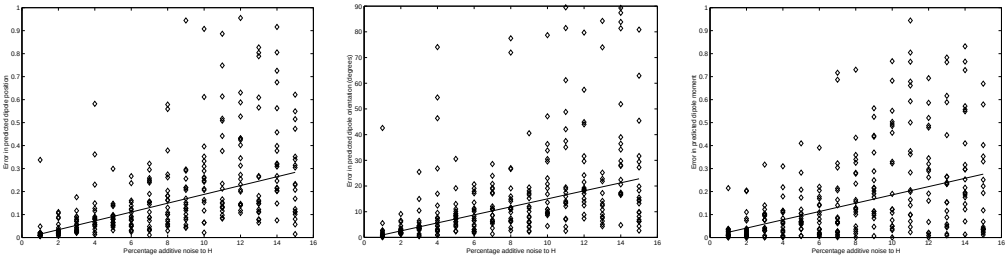

(a) Position. (b) Orientation. (c) Dipole moment.

Fig. 16. The error in predicted position, orientation and dipole moment for increasing values of measurement noise (five observer points, dipole moment unknown).

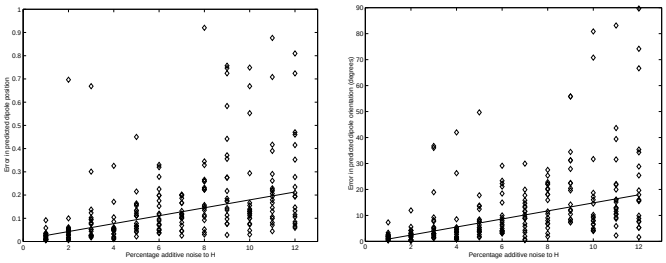

(a) Position. (b) Orientation.

Fig. 17. The error in predicted position and orientation for increasing values of measurement noise (five observer points, dipole moment known).

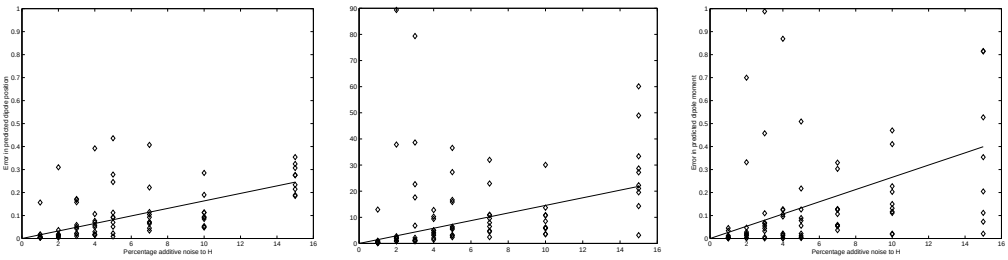

(a) Position. (b) Orientation. (c) Dipole moment.

Fig. 18. The error in predicted position, orientation and dipole moment for increasing values of measurement noise (ten observer points, dipole moment unknown).

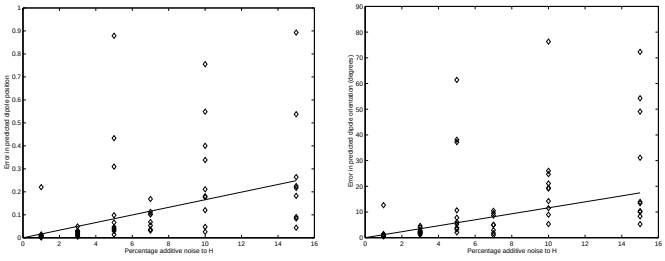

(a) Position. (b) Orientation.

Fig. 19. The error in predicted position and orientation for increasing values of measurement noise (ten observer points, dipole moment known).

APPENDIX REFERENCES

[1] C. A. Balanis, *Advanced Engineering Electromagnetics*, John Wiley & Sons, 1989.

[2] R. Plonsey and R. E. Collin, *Principles and Applications of Electromagnetic Fields*, McGraw-Hill, 1961.

[3] C. A. Balanis, *Antenna Theory Analysis and Design*, Second Edition, John Wiley & Sons, 1997.

[4] R. Gabillard, P. Degauque and J. R. Wait, "Subsurface Electromagnetic Telecommunication – A Review," *IEEE Transactions on Communications Technology*, Vol. 19, pp. 1217–1228, 1971.

[5] D. R. Vogt, *The Modelling and Design of Radio Tomography Antennas*, PhD dissertation, University of York, 2000.

[6] M. E. Mortenson, *Geomteric Modeling*, John Wiley & Sons, 1985.

[7] W. H. Press, S. A. Teukolsky, W. T. Vetterling and B. P. Flannery, *Numerical Recipes in C, The Art of Scientific Computing*, Second Edition, Cambridge University Press, 1992.

[8] J. E. Dennis and R. B. Schnabel, *Numerical Methods for Uncontrained Optimization and Nonlinear Equations*, Prentice Hall, 1983.

[9] R. M. Lishman, *A MATLAB Implementation of a Modified Newton-Raphson Algorithm to Determine the Position, Orientation and Dipole Moment of a Magnetic Dipole Antenna Buried in Rock*, Ver. 1.0, Dep of Elec. and Inf. Eng., Univ. of the Witwatersrand, 2004.

[10] R. M. Lishman, *A MATLAB Implementation of an Iterated Hill-climbing Algorithm to Determine the Position, Orientation and Dipole Moment of a Magnetic Dipole Antenna Buried in Rock*, Ver. 1.0, Dep of Elec. and Inf. Eng., Univ. of the Witwatersrand, 2004.

[11] D. E. Goldberg, *Genetic algorithms in search, optimization, and machine learning*, Addison-Wesley, 1989.

[12] D. Whitely, *A Genetic Algorithm Tutorial*, Technical Report CS-93-103, Colorado State University, 1993.

[13] R. M. Lishman, *A MATLAB Implementation of a Genetic Algorithm to Determine the Position, Orientation and Dipole Moment of a Magnetic Dipole Antenna Buried in Rock*, Ver. 1.0, Dep of Elec. and Inf. Eng., Univ. of the Witwatersrand, 2004.

[14] N. Metropolis, A. Rosenbluth, M. Rosenbluth, A. Teller and E. Teller, *Equation of state calculations for fast computing machines*, Journal of Chemical Physics, Vol. 21, pp. 1087–1092, 1953.

[15] R. M. Lishman, *A MATLAB Implementation of a Simulated Annealing Algorithm to Determine the Position, Orientation and Dipole Moment of a Magnetic Dipole Antenna Buried in Rock*, Ver. 1.0, Dep of Elec. and Inf. Eng., Univ. of the Witwatersrand, 2004.

[16] I. Mitrani, *Probabilistic Modelling*, Cambridge University Press, 1998.

[17] R. M. Lishman, *A MATLAB Routine to calculate the Cumulative Probability of a successful solution being generated by NRSOLVE*, Ver. 1.0, Dep of Elec. and Inf. Eng., Univ. of the Witwatersrand, 2004.